THE ASTROPHYSICAL JOURNAL, 329:187–207, 1988 June 1

DEEP CCD PHOTOMETRY IN GLOBULAR CLUSTERS. VII. M30

HARVEY B. RICHER[1] AND GREGORY G. FAHLMAN[1]
Department of Geophysics and Astronomy, University of British Columbia
AND
DON A. VANDENBERG
Department of Physics and Astronomy, University of Victoria
Received 1987 September 2; accepted 1987 November 17

ABSTRACT

UBV CCD photometry obtained at CFHT is discussed for the globular cluster M30 (NGC 7099, C2137−234). A single field was observed centered about 3'.4 from the cluster center (about 21 core radii). The data extend from the giant branch down to $M_V \approx 8$. The color-magnitude diagram is presented as well as the luminosity function of the cluster. The main findings of this study are as follows.

1. Even though we observed fairly close in to the cluster center, no blue stragglers nor any evidence for a binary star sequence is seen in the cluster color-magnitude diagram. Any chemical inhomogeneity among the cluster stars is limited to 0.20 dex in $[M/H]$ while the gradient between fields at 21 and 65 core radii (the latter field observed by Bolte) cannot exceed one-half this value.

2. The cluster reddening is observed to be significantly higher than that adopted in most current papers dealing with M30, $E(B-V) = 0.068 \pm 0.035$. A fit of local subdwarfs to the unevolved part of the M30 main sequence yields an apparent distance modulus of 14.85. This distance produces a rather luminous horizontal branch ($M_V = 0.35$).

3. An intercomparison of the color-magnitude diagrams of three very metal poor clusters (M15, M30, and M68) clearly shows that within the errors of the derived reddenings and distances of these clusters, there is no evidence for any age difference between them. Using a set of oxygen-enhanced isochrones, the age of M30 itself is found to be about 14 Gyr.

4. The luminosity function of M30 was determined to $M_V = 8$. Comparison of our luminosity function with one derived by Bolte at 65 core radii shows clear evidence of mass segregation in the low-mass stars, presumably through dynamical relaxation. If the mass function of the cluster is represented by a power law, then its observed slope in the 21 core radii field is ~0.0. The value measured by Bolte at 65 core radii is 1.6. These two results should differ only due to the effects of mass segregation operating on a global mass function. Mass segregation corrections, determined from multimass King-Mitchie models by Pryor, Smith, and McClure, seem to be too small to explain these different slopes.

Subject headings: clusters: globular — photometry — stars: evolution

I. INTRODUCTION AND OBSERVATIONS

There are a number of observed properties of M30 that immediately suggest that the cluster is one deserving extensive study. Integrated spectra revealed that the cluster center possessed unusually strong Balmer lines of hydrogen (Zinn and West 1984). Margon and Downes (1983) discovered a cataclysmic variable member of the cluster; one of only a few confirmed such objects in globulars. There is a central brightness cusp in M30 (King 1986) suggesting that it has a collapsed core. In the compilation of cluster properties by Webbink (1985), M30 is one of the most metal poor objects listed with $[M/H] = -2.19$.

Several photometric studies of this cluster exist. Dickens (1972) carried out photoelectric *UBV* photometry of the giant and horizontal branches and derived a reddening value of $E(B-V) = 0.06$ for the cluster. Alcaino and Liller (1980) presented photographic photometry of the cluster that did reach below the turnoff. A CCD study of the cluster has been reported by Bolte (1987*a*). This contribution produced a beautiful and tightly defined color-magnitude diagram and placed stringent limits on any metallicity variation among the stars in a given field. However, according to our results presented in § III, Bolte has underestimated the cluster reddening which has led to too small an apparent distance modulus and too large an age for the system.

Our data were obtained at CFHT in 1984 June and in 1986 August. The earlier frames were secured with the single-density RCA CCD system at the prime focus under nonphotometric conditions. This detector at CFHT provides pixels of 0''.42 on a side at the prime focus. The seeing produced images with a full width at half-maximum (FWHM) near 0''.9. Two exposures in each of *B* and *V* were obtained (each exposure lasting 900 s) and those in the same color were averaged together to produce the final frame. The M30 field was centered near star No. 89 from the list of Dickens (1972). Figure 1 displays the final *V* frame of M30 with the secondary standards marked. The 1986 August data, obtained with the double-density RCA CCD system at CFHT (0''.21 pixels), were secured mainly to calibrate the earlier data, but a short *U* exposure was added in order that the cluster reddening could be determined. The M30 data were calibrated using standards taken from Landolt (1983), the standards covering the range in spectral type from hot white

[1] Visiting Astronomer, Canada–France–Hawaii Telescope. CFHT is operated by the National Research Council of Canada, the Centre National de la Recherche Scientifique of France, and the University of Hawaii.

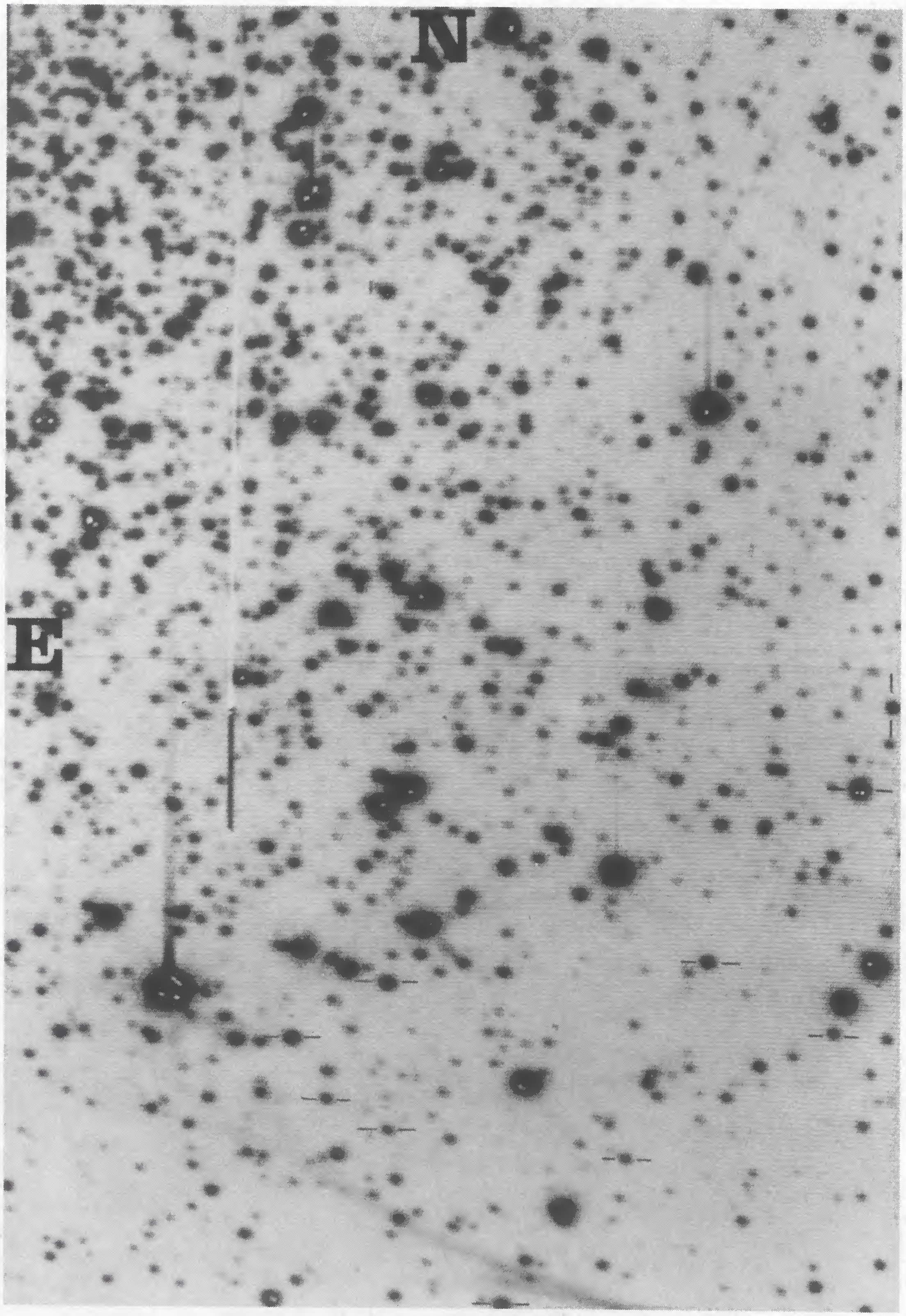

FIG. 1.—The V CCD frame of M30. The field is located about 3'.4 due west of the cluster center, with star No. 89 of Dickens (1972) roughly in the middle of the frame. The frame shown is an average of two 900 s exposures, and the objects marked are the secondary standards set up in the field (see Table 1). Pixel (0, 0) is located in the southwest corner and the X pixels increase to the east, while the Y pixels increase to the north.

TABLE 1

SECONDARY STANDARDS IN M30

X, Y	V	$B-V$	$U-B$
12, 237	18.622	0.409	−0.153
24, 206	16.475	0.644	−0.061
33, 115	19.237	0.429	...
78, 140	18.516	0.450	−0.159
105, 65	19.643	0.341	...
147, 7	18.198	0.442	−0.211
184, 73	19.728	0.330	...
184, 129	17.956	0.547	−0.129
204, 85	19.334	0.380	...
215, 108	17.828	0.575	−0.117

dwarfs to K main-sequence stars. The Landolt standards were used to set up a group of secondary standards on our frames, and the photometry of these stars is listed in Table 1. The data were reduced using standard procedures; preprocessing was done using the routines in IRAF and the analysis using DAOPHOT (Stetson 1987).

II. THE COLOR-MAGNITUDE DIAGRAM

The color-magnitude diagram (CMD) which we obtained for M30 is shown in Figure 2. All stars present on both the B and V frames that are within 1 pixel of each other (after registering the frames) and that have an error within 2.5 σ of the median error for their magnitude are included in the figure. This unbiased selection means that the stellar density along the cluster sequences represents the true luminosity function of the cluster. In total, there are 1485 stars in Figure 2. All the photometry entering into this diagram is listed in Table 2.

The turnoff of the cluster occurs at $V \approx 18.6$ and $(B-V) \approx 0.41$, values identical to that derived by Bolte (1987*a*). No blue stragglers are seen in the CMD even though our field is fairly close in to the cluster center. Also, no evidence of an approximately equal mass binary sequence is seen in the diagram. Such a sequence would make its presence known by a grouping of stars paralleling that of the main sequence, and separated from it by 0.75 mag. The cluster horizontal branch is well defined and characteristic of that of a metal-poor cluster. That is, most of the stars are concentrated to the blue side of the instability strip. The very steep giant branch and the extremely blue color of the turnoff are other indicators that the cluster is very metal poor. The metallicity estimate in the recent compilation of Webbink (1985) is $[M/H] = -2.19$.

The CMD fiducial sequence was derived by averaging the V magnitudes and $(B-V)$ colors in 0.2 mag wide bins in V and then drawing a smooth curve through the mean values obtained. The resultant smoothed main-sequence fiducial is listed in Table 3. We can use this fiducial sequence to estimate the chemical inhomogeneity among the stars in M30. Bolte (1987*a*) carried this analysis out for his fields in M30 which are located about 3 times as far as ours from the cluster center. He

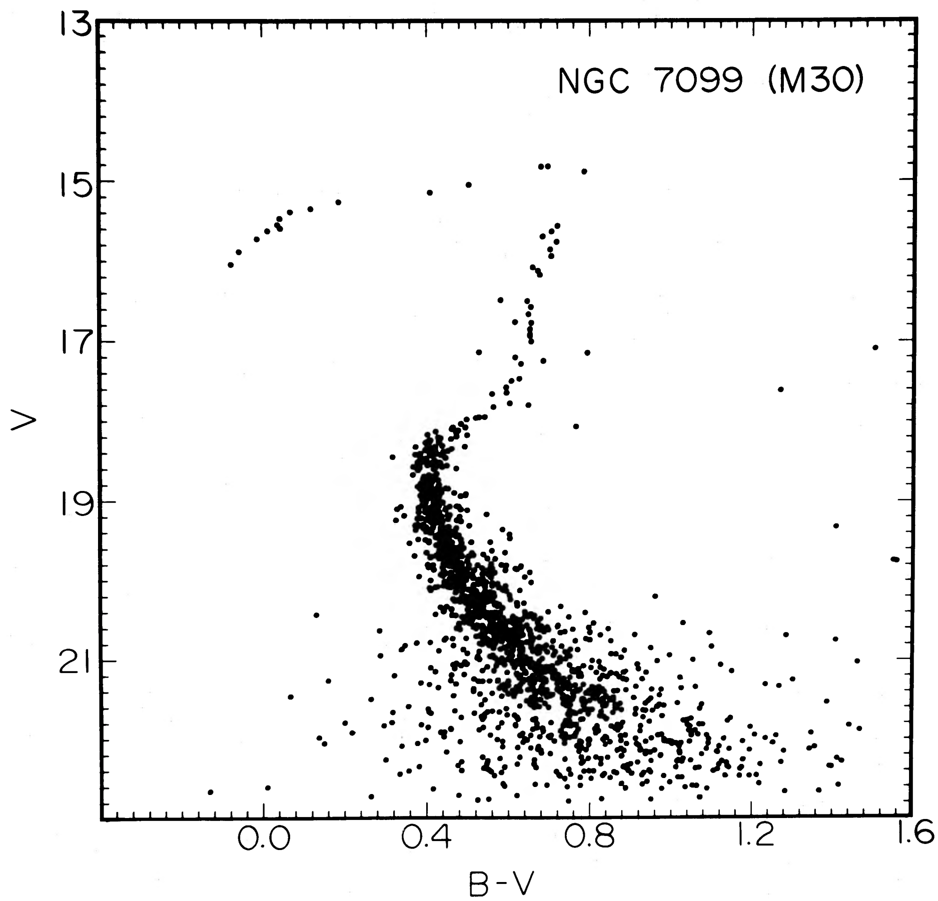

FIG. 2.—The V, $(B-V)$ color magnitude diagram of M30. There are 1485 stars in this diagram, and they represent all stars that are present on both frames and possess an error within 2.5 σ of the median error for their magnitude.

TABLE 2

Photometry of M30 Stars

X	Y	V	(B-V)	X	Y	V	(B-V)	X	Y	V	(B-V)
78.26	344.47	14.828	0.697	186.33	385.09	18.215	0.435	5.97	408.66	18.742	0.429
211.96	420.39	14.832	0.680	141.73	350.45	18.219	0.430	181.10	464.61	18.759	0.414
108.81	172.73	14.894	0.786	290.64	204.83	18.227	0.460	136.60	415.38	18.772	0.397
177.57	202.23	15.056	0.504	252.24	153.67	18.242	0.431	113.73	221.67	18.776	0.397
315.48	309.46	15.153	0.409	125.28	40.74	18.243	0.410	261.62	106.40	18.784	0.409
213.51	450.86	15.269	0.187	145.79	6.84	18.251	0.409	264.14	284.61	18.784	0.386
138.39	92.35	15.353	0.119	128.64	390.22	18.255	0.404	266.77	405.11	18.795	0.406
172.16	151.50	15.393	0.069	292.99	107.56	18.265	0.431	249.03	380.31	18.800	0.431
171.81	273.23	15.475	0.044	219.04	446.07	18.272	0.398	38.46	18.19	18.812	0.411
29.34	126.59	15.553	0.038	276.42	334.38	18.311	0.439	254.85	193.77	18.818	0.405
300.91	335.43	15.570	0.720	281.65	379.21	18.313	0.405	220.91	374.46	18.822	0.379
277.00	151.43	15.598	0.045	25.60	438.15	18.323	0.494	10.97	454.50	18.824	0.429
312.31	405.37	15.630	0.014	169.09	491.18	18.324	0.421	133.15	451.07	18.836	0.398
185.81	194.48	15.640	0.706	284.63	402.93	18.325	0.374	216.74	364.39	18.842	0.448
215.31	405.99	15.701	0.684	14.80	480.57	18.350	0.462	190.59	441.81	18.843	0.411
202.67	266.05	15.729	-0.012	162.61	430.18	18.352	0.400	290.72	447.14	18.846	0.453
283.09	299.16	15.768	0.718	149.81	255.72	18.353	0.417	242.19	48.44	18.850	0.385
125.92	44.56	15.863	0.702	199.31	282.25	18.364	0.397	214.57	437.59	18.851	0.430
208.04	336.87	15.889	-0.056	72.57	354.47	18.369	0.421	263.98	400.99	18.855	0.410
149.77	492.50	15.947	0.705	229.82	341.40	18.373	0.453	226.51	467.02	18.859	0.423
219.56	336.21	16.045	-0.076	87.15	243.62	18.382	0.418	245.46	474.41	18.862	0.436
171.89	347.12	16.086	0.659	207.34	466.66	18.383	0.407	198.59	253.41	18.866	0.425
170.53	429.45	16.130	0.672	279.59	453.55	18.391	0.442	273.09	327.36	18.867	0.423
211.82	141.26	16.181	0.677	96.89	271.26	18.407	0.385	192.07	230.90	18.871	0.397
95.00	269.45	16.492	0.581	228.94	351.65	18.408	0.424	146.44	308.07	18.885	0.398
23.94	205.84	16.505	0.646	70.21	316.86	18.420	0.409	219.55	298.09	18.887	0.391
207.52	474.94	16.580	0.655	224.21	267.67	18.421	0.373	191.78	172.92	18.895	0.414
114.90	451.39	16.670	0.649	228.92	382.55	18.426	0.409	309.62	428.65	18.895	0.409
183.75	282.25	16.767	0.616	224.21	179.16	18.427	0.416	228.25	226.62	18.896	0.437
298.71	231.61	16.777	0.656	173.79	472.37	18.427	0.436	258.12	479.58	18.902	0.468
35.80	450.08	16.858	0.653	268.43	433.32	18.452	0.318	244.57	298.54	18.906	0.421
294.46	284.95	16.923	0.653	96.70	281.15	18.459	0.385	258.92	485.54	18.915	0.497
196.97	134.26	16.941	0.653	310.52	381.68	18.463	0.447	283.49	155.41	18.917	0.406
292.43	466.35	17.012	0.656	227.24	241.63	18.473	0.399	284.69	199.37	18.920	0.409
293.52	265.67	17.096	1.502	181.29	314.68	18.479	0.396	244.62	396.47	18.930	0.496
222.63	6.89	17.146	0.529	200.16	63.64	18.494	0.399	311.24	48.15	18.935	0.385
287.94	487.06	17.155	0.794	295.28	390.18	18.496	0.419	250.99	376.01	18.942	0.484
107.60	226.87	17.211	0.617	160.01	431.37	18.514	0.390	73.44	191.13	18.944	0.421
310.58	376.43	17.256	0.686	193.92	341.70	18.519	0.379	287.00	464.23	18.948	0.431
233.25	242.17	17.293	0.631	257.03	306.81	18.522	0.431	151.74	379.81	18.959	0.396
284.93	291.32	17.478	0.627	103.23	439.34	18.527	0.434	304.11	327.65	18.965	0.407
258.21	370.75	17.506	0.608	130.07	185.76	18.533	0.410	167.94	338.17	18.988	0.390
143.70	254.75	17.585	0.595	297.07	374.17	18.544	0.431	82.58	454.25	19.009	0.431
102.47	240.91	17.615	1.268	77.75	140.03	18.555	0.403	150.98	239.47	19.020	0.398
134.04	456.54	17.653	0.596	300.13	439.04	18.560	0.450	296.82	346.16	19.021	0.440
82.08	394.53	17.665	0.561	191.65	347.28	18.576	0.368	33.62	180.74	19.022	0.418
15.17	472.21	17.783	0.604	300.77	356.91	18.577	0.439	169.85	436.46	19.033	0.418
161.97	345.81	17.808	0.649	286.18	318.70	18.579	0.423	264.11	303.56	19.052	0.390
215.46	107.52	17.829	0.564	154.88	263.32	18.586	0.384	230.83	409.02	19.068	0.430
284.11	412.07	17.953	0.543	285.75	461.79	18.594	0.418	310.53	488.58	19.070	0.474
184.03	129.33	17.956	0.529	159.54	333.53	18.598	0.473	42.28	377.06	19.071	0.416
182.36	439.52	17.965	0.521	11.65	236.63	18.602	0.418	205.73	460.77	19.072	0.479
145.23	173.41	17.984	0.499	308.93	139.75	18.614	0.380	234.08	441.14	19.073	0.457
132.92	464.36	18.037	0.485	6.96	354.33	18.615	0.380	105.99	431.99	19.076	0.338
267.10	206.39	18.075	0.766	120.80	164.11	18.662	0.425	202.60	137.73	19.085	0.381
218.73	272.78	18.082	0.465	177.76	262.11	18.678	0.367	162.97	401.56	19.089	0.410
255.32	448.88	18.084	0.496	297.06	302.29	18.679	0.406	19.77	10.16	19.090	0.419
159.13	219.12	18.102	0.462	229.37	415.66	18.696	0.414	104.65	467.96	19.092	0.417
245.33	435.32	18.121	0.478	253.56	399.87	18.698	0.394	34.35	403.86	19.093	0.448
158.25	162.00	18.133	0.423	242.25	385.26	18.708	0.419	139.61	461.61	19.094	0.400
232.84	468.77	18.146	0.473	227.38	366.34	18.712	0.396	209.74	247.32	19.094	0.412
193.93	279.94	18.171	0.403	90.02	400.44	18.722	0.405	291.65	230.13	19.104	0.398
267.60	465.41	18.180	0.500	267.80	385.00	18.725	0.406	212.50	234.98	19.104	0.329
223.77	484.23	18.196	0.474	266.74	333.34	18.727	0.406	52.73	489.06	19.109	0.447
131.53	380.74	18.206	0.429	300.01	145.80	18.732	0.392	152.84	303.31	19.110	0.484

TABLE 2—*Continued*

X	Y	V	(B-V)	X	Y	V	(B-V)	X	Y	V	(B-V)
121.82	304.56	19.110	0.424	106.36	217.04	19.396	0.437	79.83	330.52	19.651	0.400
188.31	354.31	19.114	0.414	181.45	9.28	19.402	0.410	294.47	279.53	19.656	0.511
282.07	390.32	19.119	0.500	315.99	93.59	19.404	0.469	57.75	191.73	19.657	0.430
14.00	154.31	19.123	0.412	214.06	14.30	19.411	0.435	293.51	25.74	19.661	0.468
174.72	358.20	19.127	0.407	135.71	243.67	19.411	0.447	70.87	89.26	19.665	0.482
194.57	411.80	19.130	0.416	226.03	105.73	19.415	0.452	189.54	300.48	19.668	0.437
312.51	462.49	19.132	0.419	159.14	137.39	19.421	0.464	253.46	237.86	19.675	0.539
39.79	327.34	19.138	0.405	14.75	28.22	19.422	0.456	30.42	488.51	19.686	0.515
277.39	413.94	19.141	0.397	177.83	424.09	19.423	0.603	31.70	299.74	19.688	0.455
230.98	31.76	19.142	0.381	124.15	446.63	19.425	0.440	207.16	440.74	19.689	0.453
282.82	361.65	19.142	0.431	181.82	187.91	19.426	0.430	248.23	181.96	19.692	0.371
59.49	101.33	19.168	0.418	168.71	191.11	19.429	0.429	303.50	98.93	19.692	0.423
304.93	458.70	19.171	0.547	312.58	265.83	19.435	0.479	36.74	174.61	19.694	0.465
3.95	437.35	19.177	0.429	166.36	438.23	19.438	0.456	254.90	492.10	19.696	0.431
300.92	449.16	19.179	0.452	134.45	478.32	19.443	0.423	249.78	73.64	19.698	0.487
118.24	429.90	19.179	0.457	253.16	146.64	19.445	0.472	164.70	311.40	19.699	0.503
97.80	93.54	19.186	0.409	266.91	274.33	19.453	0.450	232.23	304.16	19.703	0.503
198.20	263.35	19.187	0.346	119.55	443.88	19.461	0.423	280.75	357.50	19.704	0.444
32.99	114.84	19.191	0.423	15.44	358.82	19.472	0.439	279.81	284.34	19.705	0.455
218.82	362.64	19.192	0.410	188.36	468.84	19.475	0.604	52.15	266.24	19.706	0.461
27.55	277.70	19.193	0.432	126.02	184.17	19.478	0.452	233.83	481.97	19.706	0.412
138.02	24.16	19.198	0.437	242.73	437.17	19.484	0.380	89.05	286.15	19.710	0.453
88.84	207.55	19.198	0.406	277.98	327.48	19.486	0.484	202.19	431.18	19.712	0.409
302.33	195.96	19.200	0.481	296.96	20.95	19.492	0.397	256.33	368.27	19.717	0.457
146.01	134.41	19.217	0.416	283.52	217.15	19.497	0.452	66.13	456.56	19.717	0.475
18.24	283.16	19.217	0.436	72.32	204.03	19.499	0.446	296.33	369.54	19.725	0.431
268.64	294.62	19.217	0.409	253.09	224.55	19.508	0.434	302.70	297.61	19.725	0.549
264.26	405.70	19.220	0.387	119.23	222.31	19.509	0.406	218.82	486.25	19.730	0.447
310.01	464.54	19.222	0.378	162.83	365.75	19.510	0.446	268.15	444.10	19.731	0.568
253.06	371.00	19.230	0.453	138.69	474.84	19.521	0.510	183.73	73.33	19.739	0.472
189.82	362.96	19.232	0.400	156.50	184.23	19.521	0.444	112.35	23.28	19.743	0.449
215.00	173.53	19.237	0.436	180.05	429.64	19.522	0.556	223.25	444.85	19.743	1.549
157.24	314.03	19.238	0.404	111.77	221.24	19.523	0.406	283.49	375.65	19.752	0.473
208.94	218.33	19.240	0.418	12.07	301.07	19.525	0.462	299.31	123.04	19.752	1.557
110.71	368.09	19.243	0.326	294.20	183.55	19.525	0.443	255.96	195.56	19.757	0.447
280.89	312.49	19.245	0.474	267.24	456.27	19.531	0.486	41.49	364.56	19.758	0.453
287.51	454.64	19.258	0.485	231.79	365.21	19.531	0.359	276.57	130.21	19.759	0.500
173.52	459.46	19.261	0.439	158.16	398.06	19.533	0.449	89.58	336.01	19.761	0.462
81.60	291.99	19.266	0.411	53.58	233.40	19.541	0.453	239.89	294.70	19.770	0.466
305.86	365.36	19.274	0.423	304.25	472.54	19.547	0.459	248.47	174.15	19.780	0.449
203.93	84.60	19.298	0.437	58.67	189.75	19.548	0.452	13.32	113.71	19.785	0.484
159.88	157.32	19.300	0.392	135.53	307.44	19.551	0.436	310.98	366.71	19.787	0.477
221.12	484.82	19.301	0.378	239.78	361.13	19.558	0.424	64.97	42.46	19.789	0.442
300.80	296.38	19.308	0.373	230.06	63.58	19.560	0.434	296.59	258.63	19.789	0.462
292.90	457.10	19.315	0.505	232.21	404.66	19.560	0.446	301.23	454.65	19.799	0.558
225.61	86.52	19.319	0.379	237.66	147.49	19.561	0.444	285.11	109.22	19.805	0.403
203.63	95.07	19.322	1.406	300.72	371.01	19.564	0.457	314.79	392.98	19.806	0.583
100.17	331.44	19.328	0.455	152.89	425.20	19.565	0.446	273.31	354.63	19.808	0.486
218.20	142.24	19.331	0.452	9.65	395.26	19.576	0.461	309.83	296.94	19.809	0.504
173.30	140.50	19.335	0.399	21.95	80.59	19.587	0.479	277.61	12.67	19.810	0.416
140.00	335.74	19.336	0.416	98.48	457.97	19.595	0.469	71.43	485.37	19.810	0.525
262.05	79.26	19.340	0.435	263.48	396.68	19.595	0.491	303.24	384.13	19.814	0.595
260.04	438.66	19.344	0.473	105.05	64.89	19.596	0.446	163.28	70.41	19.819	0.477
303.69	425.87	19.348	0.393	218.57	434.25	19.596	0.477	296.22	213.36	19.821	0.456
150.80	356.84	19.348	0.399	123.38	399.66	19.599	0.489	295.12	241.84	19.822	0.631
266.72	176.58	19.358	0.442	219.55	211.50	19.606	0.487	274.34	360.92	19.823	0.465
300.96	200.87	19.364	0.586	30.11	311.90	19.624	0.450	175.86	304.07	19.823	0.466
63.01	338.43	19.369	0.374	275.57	378.20	19.627	0.431	261.52	233.36	19.832	0.440
313.13	337.30	19.376	0.435	33.06	436.68	19.628	0.481	141.08	404.19	19.834	0.630
217.35	368.76	19.380	0.407	310.70	394.35	19.629	0.560	45.18	327.43	19.835	0.405
243.20	84.01	19.384	0.412	134.67	176.88	19.640	0.460	151.72	309.09	19.837	0.439
83.34	307.58	19.387	0.400	69.23	392.51	19.643	0.452	58.44	435.62	19.842	0.472
181.10	54.43	19.389	0.469	187.60	235.39	19.645	0.466	260.84	412.08	19.844	0.503
128.43	276.43	19.391	0.460	55.61	212.60	19.651	0.462	169.18	480.57	19.849	0.556
197.45	469.38	19.396	0.448	52.25	212.07	19.651	0.592	263.08	423.80	19.849	0.536

TABLE 2—*Continued*

X	Y	V	(B-V)	X	Y	V	(B-V)	X	Y	V	(B-V)
185.60	184.87	19.852	0.561	17.72	397.03	20.066	0.490	252.42	307.89	20.262	0.552
207.53	484.91	19.855	0.617	243.95	161.85	20.066	0.515	255.22	480.39	20.264	0.469
136.91	449.58	19.860	0.474	291.89	436.08	20.069	0.561	166.88	134.03	20.264	0.539
272.38	315.54	19.863	0.621	309.81	300.02	20.069	0.471	66.84	348.52	20.268	0.482
172.20	416.51	19.867	0.496	188.02	452.12	20.072	0.593	224.97	62.35	20.271	0.547
78.72	440.45	19.868	0.489	241.66	404.74	20.073	0.442	224.78	205.91	20.273	0.536
218.56	304.47	19.870	0.474	130.49	260.77	20.076	0.465	284.26	408.60	20.274	0.509
102.31	340.13	19.870	0.418	98.90	286.40	20.082	0.543	127.61	187.95	20.277	0.516
286.73	271.18	19.873	0.517	304.35	420.16	20.083	0.427	82.10	391.04	20.281	0.504
297.13	457.93	19.877	0.593	220.47	414.79	20.085	0.453	272.29	375.80	20.285	0.566
288.49	478.91	19.878	0.549	195.78	254.32	20.089	0.422	45.07	173.03	20.286	0.621
189.74	253.84	19.883	0.477	278.34	484.15	20.090	0.577	62.64	452.33	20.287	0.496
187.31	295.83	19.889	0.552	97.02	96.94	20.091	0.459	290.05	373.02	20.289	0.638
125.71	432.90	19.894	0.442	250.88	421.19	20.097	0.407	250.14	387.66	20.291	0.570
274.83	369.77	19.901	0.653	269.29	374.09	20.102	0.484	162.59	186.89	20.302	0.518
146.35	465.93	19.905	0.567	215.09	194.77	20.116	0.502	135.10	472.39	20.303	0.577
194.98	325.22	19.908	0.459	291.48	426.17	20.119	0.478	210.72	223.79	20.307	0.567
79.92	327.70	19.914	0.446	222.59	355.50	20.119	0.586	21.00	328.55	20.309	0.527
264.54	420.33	19.920	0.537	98.33	239.17	20.125	0.590	201.96	400.95	20.321	0.509
299.85	259.47	19.921	0.499	69.80	284.61	20.128	0.410	287.03	219.31	20.322	0.622
253.86	477.41	19.926	0.552	160.65	428.37	20.131	0.628	160.19	313.90	20.323	0.573
82.08	247.33	19.928	0.509	248.60	58.07	20.132	0.595	173.57	246.35	20.324	0.505
263.70	108.56	19.930	0.485	308.43	207.76	20.134	0.487	283.35	434.37	20.331	0.729
107.04	310.70	19.930	0.435	271.78	294.00	20.135	0.521	261.18	351.19	20.333	0.449
3.00	8.81	19.934	0.511	222.72	437.92	20.139	0.543	63.40	317.19	20.333	0.539
121.14	352.70	19.940	0.462	148.38	292.34	20.150	0.471	215.50	296.50	20.339	0.530
211.42	229.38	19.940	0.481	234.70	428.20	20.150	0.555	107.81	263.29	20.341	0.434
187.03	177.06	19.940	0.492	244.08	456.63	20.152	0.512	33.81	416.91	20.341	0.530
276.96	384.43	19.941	0.440	27.48	321.29	20.153	0.522	314.40	208.83	20.349	0.586
70.45	276.99	19.947	0.500	298.09	364.35	20.163	0.564	119.77	312.46	20.353	0.521
256.47	455.33	19.951	0.382	48.45	159.68	20.170	0.541	181.07	216.82	20.361	0.461
306.59	479.23	19.958	0.475	241.88	290.90	20.177	0.539	304.16	449.66	20.366	0.500
34.53	454.69	19.959	0.489	253.91	331.58	20.181	0.521	286.74	142.77	20.368	0.461
205.67	483.61	19.961	0.640	270.39	131.03	20.188	0.548	197.35	457.88	20.381	0.442
284.86	351.06	19.962	0.558	291.72	322.19	20.189	0.603	245.32	262.29	20.383	0.539
172.27	372.65	19.964	0.514	122.01	423.82	20.191	0.534	259.49	216.90	20.389	0.536
243.17	239.12	19.964	0.494	133.42	223.45	20.193	0.529	279.65	272.08	20.394	0.442
198.88	156.43	19.967	0.468	217.96	385.60	20.195	0.540	96.78	429.60	20.398	0.541
84.51	466.28	19.972	0.514	196.27	362.53	20.197	0.487	232.63	458.06	20.398	0.640
141.32	231.87	19.976	0.491	126.39	179.91	20.197	0.547	311.58	486.25	20.399	0.698
140.16	339.38	19.981	0.457	229.70	355.72	20.198	0.566	226.75	165.23	20.400	0.521
245.87	151.47	19.985	0.468	70.74	371.82	20.201	0.537	89.48	301.50	20.402	0.522
310.10	438.44	19.986	0.537	240.29	358.47	20.203	0.565	180.65	166.52	20.405	0.580
164.35	436.44	19.987	0.464	246.96	227.97	20.204	0.494	291.44	253.00	20.408	0.567
184.52	485.41	19.994	0.528	109.68	162.36	20.204	0.961	240.56	369.50	20.408	0.789
76.70	426.14	19.996	0.486	145.89	400.44	20.212	0.512	144.11	329.69	20.409	0.515
201.10	367.39	19.997	0.497	199.75	291.04	20.212	0.505	288.00	397.07	20.409	0.537
220.74	469.05	20.000	0.527	239.46	203.80	20.230	0.543	148.51	44.03	20.410	0.507
278.81	382.92	20.002	0.410	203.10	448.07	20.231	0.554	276.25	183.74	20.412	0.558
241.83	457.83	20.010	0.530	268.98	301.17	20.236	0.535	278.72	464.48	20.412	0.550
212.25	371.06	20.013	0.471	202.22	122.55	20.237	0.465	20.38	344.14	20.420	0.553
207.26	433.49	20.021	0.444	47.50	105.46	20.238	0.527	290.62	398.82	20.420	0.503
94.59	88.97	20.022	0.474	291.53	387.16	20.243	0.548	253.05	11.76	20.420	0.552
158.23	250.00	20.022	0.462	151.31	394.86	20.244	0.605	259.78	257.78	20.421	0.560
300.60	348.97	20.024	0.545	146.36	420.02	20.245	0.545	19.31	100.16	20.421	0.512
242.86	195.43	20.029	0.656	225.66	248.34	20.245	0.504	150.63	111.53	20.423	0.655
103.71	400.66	20.036	0.561	27.44	444.18	20.248	0.477	315.02	190.85	20.423	0.541
302.27	436.00	20.043	0.574	19.35	439.90	20.248	0.492	23.56	484.40	20.424	0.537
261.55	16.97	20.047	0.527	12.94	223.17	20.250	0.482	110.59	77.73	20.428	0.527
274.98	402.62	20.048	0.540	220.48	142.68	20.250	0.556	76.50	295.94	20.428	0.564
76.48	244.69	20.048	0.460	194.07	275.56	20.251	0.530	294.67	373.48	20.429	0.422
179.15	251.00	20.057	0.486	148.96	397.20	20.251	0.479	161.67	36.51	20.432	0.131
299.02	91.48	20.057	0.459	231.96	265.39	20.253	0.502	182.57	139.91	20.432	0.524
242.23	234.44	20.060	0.515	126.82	426.78	20.257	0.486	309.93	418.38	20.436	0.578
202.49	346.09	20.063	0.455	36.98	334.96	20.260	0.515	248.83	41.98	20.440	0.462

TABLE 2—*Continued*

X	Y	V	(B-V)	X	Y	V	(B-V)	X	Y	V	(B-V)
246.13	333.38	20.441	0.503	185.77	410.59	20.582	0.721	262.12	35.12	20.691	0.580
301.16	236.90	20.441	0.656	184.31	471.30	20.585	0.589	163.90	361.36	20.699	0.630
54.39	219.46	20.442	0.558	107.12	413.42	20.588	0.515	122.74	389.92	20.699	0.529
312.19	470.21	20.442	0.471	289.43	456.22	20.589	0.696	239.35	299.77	20.702	0.566
259.43	399.99	20.442	0.664	275.48	460.76	20.594	0.798	298.25	27.91	20.703	0.573
154.20	348.76	20.445	0.541	193.01	416.83	20.595	0.555	299.18	130.77	20.707	0.521
188.46	48.16	20.446	0.658	8.35	182.83	20.597	0.634	253.68	471.26	20.709	0.592
300.24	308.05	20.446	0.641	112.44	378.85	20.598	0.556	31.88	233.52	20.709	0.570
139.97	413.53	20.447	0.517	286.88	431.42	20.600	0.672	115.00	471.19	20.712	0.541
278.11	417.98	20.450	0.498	287.33	386.78	20.601	0.540	106.82	49.76	20.716	0.593
307.63	237.27	20.456	0.611	290.86	85.47	20.606	0.473	130.90	492.53	20.720	0.676
278.88	239.60	20.456	0.523	311.31	134.64	20.607	0.537	250.40	448.38	20.722	0.617
144.92	149.01	20.456	0.553	122.51	435.25	20.607	0.673	181.45	458.95	20.724	0.537
131.07	108.11	20.459	0.487	17.30	264.75	20.608	0.521	271.37	487.28	20.725	0.656
298.05	257.11	20.459	0.648	305.06	289.66	20.610	0.846	40.02	193.77	20.726	0.621
63.51	401.42	20.462	0.529	234.36	459.59	20.610	0.676	79.70	198.25	20.731	0.497
192.04	434.90	20.463	0.749	116.85	422.19	20.611	0.670	168.63	303.15	20.731	0.661
85.06	363.49	20.467	0.548	80.90	443.26	20.612	0.578	263.60	385.02	20.732	0.447
241.09	310.60	20.469	0.489	274.31	322.86	20.614	0.617	50.79	15.86	20.733	0.574
191.55	396.80	20.471	0.575	199.40	371.63	20.619	0.759	266.25	56.53	20.736	0.464
105.50	300.58	20.475	0.587	195.61	111.30	20.620	0.651	55.76	286.33	20.737	0.622
152.17	411.87	20.478	0.554	56.17	365.78	20.621	0.592	308.01	122.08	20.737	0.791
137.91	238.76	20.479	0.560	280.46	393.22	20.621	0.482	178.93	323.21	20.738	0.575
287.15	394.87	20.480	0.663	118.95	297.88	20.623	0.699	309.09	368.53	20.738	0.547
253.30	266.56	20.481	0.679	142.99	289.41	20.625	0.677	97.10	223.00	20.744	0.610
290.82	403.38	20.482	0.617	81.81	325.27	20.627	0.573	205.28	434.33	20.748	0.571
161.06	225.40	20.492	0.634	250.24	365.62	20.629	0.597	105.61	447.65	20.749	1.407
304.55	223.70	20.495	0.622	4.57	273.85	20.630	0.653	242.68	311.86	20.751	0.802
9.39	266.38	20.500	0.562	89.80	193.15	20.631	0.571	126.98	464.34	20.752	0.444
254.48	388.22	20.503	0.511	177.35	178.52	20.632	0.604	144.67	201.83	20.753	0.584
57.02	479.65	20.514	0.498	120.31	69.86	20.633	0.610	40.86	452.05	20.754	0.575
21.97	53.87	20.515	0.600	151.09	302.19	20.633	0.286	306.22	321.00	20.755	0.602
181.08	264.88	20.517	0.606	247.54	244.72	20.636	0.584	179.69	415.85	20.762	0.659
60.20	372.68	20.518	0.558	118.92	492.94	20.638	0.539	249.48	457.35	20.763	0.852
102.65	115.76	20.521	0.583	151.10	330.41	20.638	0.554	275.73	490.23	20.765	0.765
228.21	264.36	20.528	0.509	281.09	183.04	20.638	0.602	288.30	196.05	20.765	0.556
165.70	88.26	20.530	0.492	185.57	402.09	20.644	0.631	157.45	447.09	20.766	0.710
291.96	479.64	20.533	0.611	182.55	32.98	20.646	0.595	117.85	319.75	20.774	0.584
130.67	410.92	20.534	0.672	133.23	491.05	20.648	0.688	38.78	303.19	20.775	0.610
84.40	136.01	20.535	0.590	133.10	249.96	20.648	0.739	113.23	375.78	20.776	0.570
263.64	490.36	20.535	1.029	35.63	312.63	20.651	0.593	171.68	252.67	20.778	0.545
189.54	160.18	20.536	0.562	280.81	479.27	20.654	0.579	91.76	397.13	20.782	0.645
202.33	166.55	20.540	0.810	199.02	355.05	20.656	0.583	310.53	39.33	20.783	0.548
200.38	238.44	20.541	0.505	141.33	355.82	20.657	0.562	258.00	82.52	20.784	0.409
288.42	381.21	20.541	0.627	304.15	360.40	20.657	0.801	275.94	205.96	20.787	0.554
173.12	312.97	20.544	0.479	263.61	391.10	20.657	0.589	121.90	258.07	20.789	0.627
33.42	456.25	20.547	0.560	152.59	429.30	20.659	0.728	271.56	448.75	20.790	0.376
235.40	159.25	20.549	0.577	17.37	354.73	20.662	0.614	282.50	186.59	20.791	0.631
258.78	481.72	20.550	0.615	209.70	294.72	20.662	1.094	218.31	217.66	20.796	0.611
173.63	412.76	20.564	0.578	254.55	200.87	20.665	0.600	269.67	471.30	20.796	0.530
272.46	199.81	20.565	0.645	257.85	407.88	20.665	0.628	39.42	25.77	20.806	0.567
143.45	277.50	20.565	0.628	251.69	458.41	20.666	0.591	126.90	208.42	20.807	0.621
48.87	195.33	20.565	0.523	279.10	275.23	20.670	0.542	13.21	447.54	20.807	0.656
273.64	120.44	20.567	0.558	190.46	323.02	20.671	0.602	297.35	238.08	20.808	0.536
263.33	377.00	20.567	0.555	265.63	316.14	20.675	0.606	20.93	357.27	20.811	0.624
253.68	247.27	20.568	0.722	174.07	41.97	20.677	0.655	99.62	284.08	20.817	0.553
167.15	357.77	20.569	0.524	47.35	278.70	20.679	0.535	283.27	466.37	20.819	0.553
205.96	250.69	20.571	0.578	158.27	297.28	20.681	0.570	201.44	343.26	20.820	0.693
282.27	462.12	20.571	0.479	293.81	236.48	20.685	0.911	257.41	460.82	20.822	0.466
263.35	30.25	20.571	0.536	230.34	477.83	20.688	0.827	222.52	375.99	20.823	0.348
131.79	426.33	20.578	0.521	212.40	309.19	20.688	0.593	167.51	471.28	20.824	0.611
220.55	169.89	20.578	0.571	44.35	472.12	20.688	0.620	182.74	299.36	20.827	0.600
170.31	451.49	20.578	0.523	282.64	80.88	20.689	1.284	197.82	304.33	20.831	0.731
83.59	99.74	20.579	0.681	145.82	436.40	20.689	0.655	107.87	396.06	20.832	1.100
16.83	407.07	20.580	0.592	141.37	400.64	20.690	0.636	24.10	377.08	20.835	0.674

TABLE 2—*Continued*

X	Y	V	(B-V)	X	Y	V	(B-V)	X	Y	V	(B-V)
157.90	491.36	20.842	0.656	306.48	69.85	21.013	0.807	250.62	156.04	21.156	0.677
209.89	361.22	20.846	0.685	180.12	245.11	21.015	0.966	290.35	189.91	21.157	0.763
241.84	98.38	20.847	0.708	71.73	412.10	21.016	0.622	245.51	370.07	21.158	0.884
61.33	60.84	20.849	0.633	198.55	401.01	21.017	0.653	209.47	60.36	21.160	0.939
284.90	192.73	20.849	0.590	221.27	379.83	21.019	0.646	199.18	412.99	21.161	0.597
256.68	444.77	20.849	0.950	78.86	473.86	21.020	0.579	308.87	247.52	21.164	0.817
260.11	295.33	20.849	0.672	110.58	156.47	21.022	0.676	159.96	39.75	21.166	0.679
295.59	492.52	20.852	0.590	61.63	463.24	21.025	0.824	309.17	233.85	21.168	0.853
299.54	417.18	20.852	0.609	69.46	416.90	21.028	1.461	198.72	191.53	21.168	0.643
260.04	260.91	20.857	0.564	291.76	383.06	21.029	0.728	252.53	319.99	21.173	0.674
205.20	62.12	20.859	0.688	199.37	428.67	21.030	0.494	95.20	98.51	21.174	0.851
233.11	171.22	20.860	0.611	136.38	423.57	21.032	0.587	64.58	324.95	21.176	0.620
254.21	180.67	20.865	0.635	144.75	110.87	21.041	0.615	298.41	396.51	21.179	0.866
167.58	368.73	20.867	0.581	234.53	12.89	21.042	0.655	95.65	177.64	21.180	0.778
225.98	90.74	20.869	0.490	296.31	424.79	21.045	0.574	118.52	427.83	21.187	0.492
268.49	111.01	20.871	0.753	165.94	413.95	21.045	0.721	161.93	139.96	21.194	0.622
262.22	463.42	20.871	0.340	216.51	315.37	21.047	0.473	251.21	189.01	21.194	0.461
172.35	462.30	20.875	0.771	116.25	271.65	21.048	0.645	171.97	398.28	21.195	0.723
221.56	304.99	20.878	0.628	109.50	364.82	21.049	0.661	297.04	292.98	21.199	0.322
229.28	249.07	20.881	0.886	229.40	284.11	21.049	0.610	35.65	283.74	21.202	0.629
149.19	232.70	20.881	0.611	299.14	456.91	21.050	0.622	147.85	7.92	21.203	0.833
279.09	421.40	20.888	0.430	142.25	307.93	21.055	0.629	55.53	375.84	21.205	0.660
99.57	475.94	20.895	0.671	244.50	228.26	21.056	0.499	309.25	132.26	21.213	0.774
170.77	360.66	20.895	0.635	265.21	439.08	21.056	0.917	220.90	244.22	21.214	0.780
135.06	373.84	20.897	0.660	219.30	437.36	21.061	0.465	290.55	474.33	21.216	0.844
223.00	465.36	20.897	0.529	180.98	174.84	21.063	1.122	227.61	38.75	21.217	0.677
20.13	484.78	20.903	0.715	132.44	356.27	21.070	0.591	216.32	232.53	21.218	0.710
138.62	431.11	20.903	0.740	200.07	255.85	21.071	0.485	48.11	485.78	21.219	0.873
44.61	240.60	20.906	0.696	193.52	414.66	21.073	0.751	194.11	399.52	21.221	1.022
17.87	474.87	20.913	0.597	290.71	278.32	21 079	0.571	78.04	165.69	21.223	0.660
285.76	27.43	20.915	0.676	239.21	155.05	21.081	0.785	259.54	421.12	21.227	0.752
215.71	300.04	20.919	0.500	169.75	238.99	21.083	0.666	231.39	165.67	21.236	0.627
208.37	319.01	20.923	0.672	288.32	468.99	21.084	0.708	295.24	126.07	21.237	0.710
180.98	372.87	20.925	0.853	63.75	273.48	21.092	0.693	88.01	434.62	21.238	0.686
160.95	236.41	20.925	0.604	276.32	390.07	21.094	0.549	249.36	64.40	21.243	0.929
108.20	401.09	20.928	0.746	113.56	368.13	21.094	0.674	283.84	22.39	21.244	0.883
271.20	173.42	20.929	0.865	251.80	403.53	21.095	0.655	4.11	243.83	21.244	0.736
49.90	388.69	20.931	0.629	232.00	299.37	21.096	0.702	209.83	18.53	21.245	0.651
86.26	493.43	20.941	0.996	194.58	370.78	21.097	0.681	60.64	242.01	21.246	0.516
64.76	281.28	20.945	0.562	79.93	80.54	21.099	0.827	235.77	153.88	21.246	0.676
256.14	37.08	20.948	0.288	251.55	95.13	21.100	0.615	139.50	442.59	21.247	0.826
118.81	236.01	20.950	0.711	133.35	377.54	21.102	0.681	20.24	215.86	21.250	1.301
226.22	360.41	20.952	0.628	245.50	405.74	21.102	0.410	186.88	467.51	21.252	0.720
19.23	249.59	20.953	0.609	257.57	327.63	21.103	0.701	107.79	446.86	21.253	0.891
255.00	291.88	20.959	0.752	161.48	99.83	21.103	0.804	257.81	412.89	21.256	0.681
215.10	52.34	20.959	0.555	107.08	470.03	21.106	0.684	274.98	244.13	21.256	0.692
164.71	142.38	20.960	0.525	314.54	119.15	21.110	0.635	77.94	391.41	21.257	0.664
164.57	329.32	20.961	0.558	269.05	447.07	21.111	0.469	46.24	352.16	21.259	0.640
59.20	272.97	20.969	0.642	256.14	352.08	21.116	0.920	153.84	404.34	21.260	0.575
244.73	307.72	20.971	0.878	170.99	22.62	21.120	0.773	46.47	416.73	21.263	0.459
105.86	380.42	20.978	0.524	132.77	22.92	21.122	0.836	106.09	396.61	21.264	0.160
126.40	309.05	20.979	0.727	55.73	461.48	21.126	0.666	222.51	283.99	21.267	0.728
239.32	169.05	20.981	0.630	293.64	157.51	21.132	0.758	128.95	445.76	21.267	0.726
257.14	427.14	20.981	0.568	119.00	489.13	21.141	0.537	93.71	208.74	21.271	0.659
120.13	378.33	20.985	0.584	194.22	300.16	21.141	0.766	155.02	398.98	21.272	0.554
274.33	171.03	20.987	0.602	54.37	346.82	21.142	0.565	178.53	171.33	21.273	0.600
179.73	422.61	20.992	0.683	107.08	421.13	21.142	1.150	306.94	12.25	21.274	0.527
131.85	188.44	20.993	0.741	67.96	275.49	21.143	0.714	254.11	187.03	21.275	0.537
148.74	335.66	20.995	0.654	313.91	241.60	21.149	0.758	104.20	19.73	21.283	0.692
203.02	369.48	20.996	0.599	152.61	8.79	21.151	0.676	197.95	454.18	21.284	0.636
313.69	342.35	20.998	0.530	260.23	286.91	21.152	0.422	289.06	353.34	21.289	0.386
289.31	286.84	20.999	1.054	99.81	447.63	21.154	0.692	278.93	282.19	21.296	0.663
25.06	242.49	21.002	0.634	243.85	424.30	21.154	0.688	244.20	342.75	21.297	0.747
13.65	430.48	21.011	0.606	48.66	303.31	21.155	0.641	66.79	202.98	21.304	0.654
278.31	257.37	21.012	0.636	113.46	185.16	21.155	0.705	29.26	172.21	21.306	0.720

TABLE 2—*Continued*

X	Y	V	(B-V)	X	Y	V	(B-V)	X	Y	V	(B-V)
261.66	457.73	21.307	0.472	168.58	14.62	21.426	0.792	153.56	436.78	21.567	0.654
295.58	474.04	21.309	1.233	253.74	294.37	21.426	0.760	73.14	271.80	21.568	0.972
253.99	305.78	21.311	0.407	147.69	119.65	21.428	0.683	292.54	320.33	21.572	0.534
303.22	57.64	21.313	0.630	87.08	228.74	21.433	0.801	175.93	111.51	21.574	0.842
263.34	315.82	21.319	0.785	120.44	419.32	21.434	0.600	119.24	255.81	21.575	0.864
76.36	415.80	21.319	0.659	189.99	54.64	21.435	0.531	248.35	252.40	21.576	0.668
213.88	191.46	21.319	0.590	82.03	30.49	21.441	0.666	303.21	477.73	21.576	0.753
228.26	292.39	21.320	0.736	21.77	2.98	21.444	0.709	129.82	52.12	21.577	0.658
245.06	419.21	21.327	0.765	115.66	459.97	21.444	0.702	298.39	171.32	21.580	0.983
195.80	288.48	21.328	0.600	281.61	323.02	21.447	0.972	182.84	231.88	21.580	0.785
255.90	297.87	21.333	1.267	241.34	427.64	21.449	0.696	308.33	260.96	21.581	0.742
37.41	439.21	21.334	0.683	256.49	238.65	21.451	0.701	184.43	86.07	21.587	0.628
155.46	36.87	21.334	0.584	16.42	90.12	21.452	0.734	169.39	79.07	21.587	0.840
204.01	350.76	21.337	0.628	196.14	165.46	21.456	0.819	254.79	463.65	21.589	0.356
243.55	281.23	21.340	0.753	201.07	183.46	21.456	0.466	160.01	300.26	21.590	0.834
180.89	488.01	21.341	1.060	63.48	56.39	21.457	0.703	111.50	310.78	21.597	0.676
268.42	187.43	21.341	0.914	144.21	317.27	21.458	0.698	257.25	262.63	21.598	0.966
168.85	11.44	21.344	0.807	99.27	136.46	21.459	0.695	126.74	361.52	21.601	0.664
89.80	97.14	21.346	0.620	314.72	274.65	21.463	0.584	114.36	236.71	21.604	0.699
300.00	254.31	21.346	0.824	205.72	52.06	21.464	0.067	4.32	210.22	21.610	0.864
250.29	312.93	21.351	0.429	205.37	373.93	21.465	0.841	172.54	439.21	21.617	1.071
294.47	138.96	21.355	1.025	30.65	52.92	21.467	0.614	164.10	319.79	21.618	0.867
41.93	441.49	21.356	0.681	195.71	295.21	21.470	0.761	75.21	487.51	21.620	0.595
278.46	64.23	21.359	0.660	155.84	372.49	21.471	0.695	313.05	13.44	21.620	0.404
314.71	257.51	21.361	0.578	187.83	444.35	21.478	0.859	188.75	95.14	21.628	0.914
150.68	210.06	21.363	0.814	64.62	128.57	21.479	0.745	310.68	182.19	21.630	0.790
180.49	410.39	21.369	0.734	100.07	461.51	21.480	0.745	187.84	476.96	21.633	0.807
109.39	40.92	21.370	0.515	9.72	480.32	21.480	0.811	256.43	183.60	21.635	0.799
242.79	274.78	21.370	0.721	225.23	232.77	21.483	0.656	13.02	191.04	21.638	0.879
215.30	275.65	21.371	0.749	182.92	162.76	21.483	0.909	23.63	368.10	21.642	0.932
130.02	394.52	21.373	0.832	57.20	360.89	21.490	0.951	301.23	323.10	21.643	0.751
226.36	425.66	21.375	0.976	15.87	349.24	21.491	0.815	248.80	199.87	21.645	0.469
281.46	258.73	21.375	0.829	218.23	188.18	21.491	0.733	290.38	378.89	21.646	0.938
264.14	413.70	21.375	0.953	276.95	446.09	21.497	0.265	144.51	3.08	21.648	0.955
70.88	16.17	21.377	0.655	198.60	210.70	21.499	0.833	226.67	59.50	21.651	0.561
222.73	241.71	21.381	0.592	25.45	327.50	21.499	0.851	268.80	99.85	21.657	0.778
162.32	233.71	21.382	0.720	56.19	257.18	21.499	0.785	212.45	385.55	21.659	0.406
290.96	307.94	21.382	0.777	204.52	390.66	21.500	0.782	289.52	114.85	21.661	0.549
90.30	52.84	21.383	0.648	255.20	410.56	21.501	0.663	306.67	203.72	21.662	0.578
167.35	366.87	21.384	0.695	310.12	24.59	21.502	0.754	288.71	111.96	21.662	0.829
144.56	189.14	21.385	0.890	239.34	15.71	21.504	0.758	86.72	234.28	21.662	0.318
244.50	388.14	21.388	0.807	63.61	448.52	21.507	0.679	60.86	432.42	21.669	0.761
266.34	361.74	21.389	0.828	301.68	313.07	21.508	0.668	58.03	94.61	21.673	0.858
43.64	177.72	21.392	0.689	160.14	403.01	21.509	0.543	118.73	303.11	21.674	0.411
114.17	214.99	21.392	0.610	132.96	352.31	21.511	0.859	220.60	317.86	21.675	0.517
305.98	233.65	21.393	0.819	22.04	441.96	21.517	0.851	239.39	279.41	21.682	0.766
179.03	94.24	21.394	0.869	275.88	438.25	21.521	0.782	127.69	373.67	21.686	0.797
55.56	307.46	21.396	0.799	279.58	486.46	21.521	0.945	145.56	443.66	21.687	0.753
150.25	217.07	21.397	0.773	195.03	327.87	21.522	0.801	307.88	161.14	21.689	0.542
233.60	465.75	21.398	0.860	147.87	314.61	21.522	0.645	73.30	456.77	21.690	0.746
127.20	436.26	21.399	0.813	26.10	264.15	21.524	0.829	111.68	332.47	21.698	0.913
307.34	470.48	21.399	0.515	245.37	283.40	21.525	0.748	160.81	451.97	21.699	0.597
115.05	80.31	21.401	0.630	261.82	339.68	21.525	0.834	299.67	242.68	21.703	0.615
29.24	251.40	21.403	0.674	246.24	352.63	21.532	0.827	145.42	352.41	21.716	0.826
117.00	410.44	21.407	0.837	230.55	214.48	21.534	1.386	99.86	384.56	21.716	0.751
284.89	172.51	21.408	0.763	145.86	105.63	21.541	0.785	196.20	231.58	21.717	0.979
167.75	315.73	21.409	0.764	233.77	21.53	21.542	0.656	149.26	245.04	21.719	0.534
156.21	404.72	21.409	0.727	174.94	367.20	21.547	1.016	82.59	285.62	21.725	0.836
224.89	229.69	21.409	0.666	277.29	456.57	21.554	0.789	246.75	414.85	21.728	0.541
290.99	31.27	21.410	0.797	230.93	472.22	21.554	0.938	266.51	265.41	21.729	0.485
185.97	298.01	21.411	0.666	292.08	7.27	21.555	0.664	79.89	90.77	21.729	0.621
144.25	395.35	21.418	0.824	249.65	230.95	21.557	0.690	223.05	276.33	21.731	0.932
25.00	239.81	21.425	0.617	18.33	461.85	21.559	0.735	303.66	67.58	21.734	1.147
201.84	290.04	21.426	0.561	186.36	98.92	21.560	0.876	140.93	432.00	21.745	1.050
80.93	471.00	21.426	0.801	292.15	405.81	21.561	1.076	252.60	348.03	21.746	0.667

TABLE 2—*Continued*

X	Y	V	(B-V)	X	Y	V	(B-V)	X	Y	V	(B-V)
84.76	105.51	21.752	0.842	312.65	479.02	21.920	0.218	112.79	159.59	22.057	0.378
264.25	179.19	21.754	0.537	279.14	469.18	21.925	1.348	57.65	331.66	22.058	1.093
217.37	122.60	21.754	0.784	130.63	60.02	21.927	0.767	198.49	293.72	22.064	0.892
288.29	273.98	21.754	0.624	230.22	322.63	21.931	0.816	166.08	383.17	22.066	1.003
2.86	113.58	21.757	0.779	24.63	400.16	21.932	0.635	110.25	67.85	22.068	0.917
274.55	365.14	21.758	0.660	44.57	299.11	21.941	0.740	192.70	487.92	22.071	0.839
283.76	480.65	21.763	1.040	37.84	332.12	21.948	1.207	92.39	450.04	22.073	0.798
259.50	343.17	21.770	1.140	151.51	131.82	21.949	0.978	124.61	339.37	22.085	0.772
219.39	281.92	21.770	1.031	286.33	254.10	21.949	1.068	300.16	401.96	22.086	0.922
233.08	62.64	21.772	0.741	294.41	161.84	21.954	0.556	45.52	62.17	22.088	0.769
138.29	194.80	21.781	0.751	135.33	408.92	21.956	0.705	154.66	302.37	22.089	0.340
183.92	293.73	21.788	0.948	297.96	490.58	21.956	1.089	227.63	481.57	22.094	1.021
251.54	236.92	21.791	0.316	117.13	418.48	21.956	1.051	270.93	245.78	22.096	0.674
224.00	106.99	21.794	0.201	256.74	405.23	21.956	0.969	188.42	492.33	22.097	1.120
88.38	170.08	21.796	0.705	293.47	166.49	21.957	0.655	229.53	372.18	22.102	1.357
219.85	254.18	21.798	0.882	59.20	243.30	21.957	1.260	117.53	333.95	22.102	0.586
199.27	395.54	21.800	0.584	212.30	221.24	21.958	0.628	112.20	315.52	22.110	0.623
168.50	218.67	21.809	0.670	230.37	77.25	21.958	0.889	113.59	331.70	22.114	0.655
300.05	117.17	21.817	1.079	54.62	247.84	21.967	0.731	297.45	487.68	22.114	0.780
305.51	242.17	21.818	1.070	59.96	477.05	21.967	0.877	82.35	437.52	22.126	0.878
314.29	289.49	21.819	0.387	200.03	120.83	21.968	0.761	292.74	181.31	22.129	1.145
262.89	478.12	21.821	0.767	276.43	194.61	21.969	0.699	49.13	207.16	22.129	0.672
66.92	366.23	21.822	0.747	52.17	392.26	21.969	0.764	122.81	419.48	22.131	1.344
189.45	422.48	21.823	0.761	205.23	275.84	21.974	0.677	54.22	443.78	22.131	1.089
134.57	421.99	21.824	0.617	189.74	70.93	21.975	0.839	117.80	62.61	22.136	0.927
109.19	207.68	21.824	0.869	280.57	435.09	21.975	0.443	67.13	211.96	22.138	0.792
226.29	220.44	21.825	0.755	257.29	77.12	21.980	0.137	53.84	245.72	22.140	1.195
254.97	322.88	21.826	1.041	85.35	189.71	21.982	0.751	293.79	128.95	22.142	0.869
228.65	443.11	21.831	1.442	107.86	253.60	21.983	0.702	265.42	84.10	22.145	0.680
242.33	417.00	21.831	0.297	297.67	206.60	21.986	0.842	57.73	137.90	22.147	0.925
243.88	36.68	21.833	0.747	190.68	80.68	21.992	1.234	84.30	450.31	22.147	0.961
176.51	328.58	21.835	0.618	250.44	242.41	21.995	0.953	151.27	188.76	22.152	0.886
165.84	327.92	21.836	0.735	184.59	404.45	21.998	0.914	270.00	240.15	22.156	1.280
197.69	111.89	21.837	0.754	118.65	362.31	22.001	1.131	60.98	172.37	22.156	0.774
85.27	215.34	21.837	0.871	143.26	383.48	22.002	0.640	266.26	226.45	22.160	1.022
22.47	210.61	21.842	0.926	68.80	75.46	22.005	1.094	52.67	175.45	22.163	0.940
174.53	93.42	21.842	0.819	283.28	106.34	22.005	0.799	265.03	79.80	22.164	0.449
139.58	29.05	21.844	0.854	286.38	57.19	22.007	0.984	285.38	53.52	22.165	1.114
15.98	414.49	21.844	1.047	284.65	177.37	22.009	0.738	182.28	257.99	22.168	1.023
310.37	124.02	21.848	1.196	139.79	295.34	22.009	0.834	218.92	184.01	22.169	1.116
11.79	90.36	21.851	0.404	80.65	289.39	22.009	0.573	303.77	304.31	22.172	0.950
116.09	336.95	21.856	0.877	286.57	214.59	22.012	0.797	244.03	469.69	22.178	0.681
225.62	117.71	21.856	0.539	36.84	171.46	22.015	0.801	194.79	407.60	22.186	1.023
294.56	143.35	21.859	0.575	256.89	233.13	22.018	0.646	154.20	267.51	22.186	0.703
178.75	380.14	21.860	0.670	177.80	235.80	22.018	0.398	72.59	426.57	22.193	0.938
258.34	203.76	21.865	0.684	282.67	50.56	22.027	0.878	46.49	165.98	22.199	1.077
224.99	54.10	21.867	0.459	119.79	140.19	22.029	0.713	161.62	384.97	22.206	0.976
294.23	187.42	21.872	0.864	77.17	401.58	22.031	0.776	245.21	399.18	22.216	0.975
117.42	227.79	21.876	0.814	8.37	73.42	22.032	1.178	156.10	469.48	22.219	1.629
278.18	363.96	21.879	0.660	55.00	178.40	22.032	0.997	252.15	183.99	22.220	0.879
277.61	168.24	21.879	0.460	65.63	94.41	22.033	0.984	151.95	118.09	22.230	0.816
129.98	228.43	21.881	0.772	213.85	305.76	22.033	0.586	305.41	384.75	22.231	0.537
243.57	191.74	21.885	1.468	289.04	320.59	22.035	0.482	183.10	409.36	22.231	0.780
309.81	27.70	21.889	0.529	104.83	270.88	22.037	1.047	14.85	215.86	22.233	0.628
313.50	99.93	21.895	0.870	42.66	294.74	22.038	0.993	159.42	455.56	22.234	0.845
297.83	360.51	21.897	1.060	91.07	372.77	22.038	1.003	55.85	440.56	22.245	0.797
245.15	382.12	21.898	0.729	67.89	47.96	22.039	0.939	307.66	294.94	22.248	1.413
9.72	340.36	21.899	1.045	201.08	158.44	22.040	0.780	163.34	262.67	22.249	0.580
52.36	352.31	21.901	0.823	69.18	94.66	22.041	0.851	266.90	339.16	22.252	0.828
149.55	346.02	21.902	0.820	280.26	208.65	22.044	0.636	22.70	423.54	22.253	1.031
129.39	424.69	21.903	0.686	98.42	247.31	22.049	1.253	91.43	437.86	22.256	0.739
66.80	423.53	21.906	0.817	58.24	445.89	22.053	1.026	221.81	323.37	22.262	0.301
308.61	187.10	21.907	0.925	258.15	462.59	22.055	0.150	186.63	361.06	22.263	0.664
252.11	428.57	21.914	0.444	234.45	253.03	22.056	0.738	229.13	298.51	22.264	1.179
138.63	140.75	21.916	0.435	17.15	248.43	22.057	1.013	237.28	122.52	22.272	1.019

TABLE 2—*Continued*

X	Y	V	(B-V)	X	Y	V	(B-V)	X	Y	V	(B-V)
222.19	199.64	22.274	1.050	269.76	192.53	22.387	1.116	303.39	193.06	22.566	0.587
315.50	158.98	22.276	0.550	292.60	149.95	22.394	0.553	77.62	59.25	22.571	0.666
111.13	384.37	22.279	0.952	111.53	64.63	22.396	0.947	32.37	243.46	22.574	0.930
112.43	388.89	22.283	1.016	96.57	211.28	22.399	0.486	122.55	207.87	22.581	0.695
56.05	161.64	22.283	1.127	277.23	107.70	22.402	0.799	234.21	433.39	22.583	0.777
246.72	5.44	22.285	1.425	224.68	26.09	22.403	0.357	94.66	471.34	22.589	1.417
244.38	235.59	22.287	0.486	76.68	218.40	22.404	0.897	178.71	77.90	22.592	1.054
203.27	249.43	22.287	0.784	227.17	171.41	22.404	0.810	22.43	248.01	22.595	1.065
244.52	347.93	22.291	1.028	66.13	403.59	22.405	0.786	287.29	328.40	22.596	0.591
168.61	377.16	22.297	0.919	268.81	270.75	22.409	1.106	17.59	488.34	22.602	0.745
48.11	285.71	22.297	1.274	270.95	222.53	22.410	0.718	172.21	222.91	22.606	0.011
108.73	485.12	22.304	1.139	218.60	118.56	22.413	0.558	175.71	388.84	22.611	1.036
244.44	23.06	22.306	0.780	205.33	234.42	22.415	0.860	189.32	377.50	22.617	0.889
194.79	357.74	22.313	0.548	159.09	230.75	22.421	0.951	51.97	33.04	22.628	1.090
33.47	355.85	22.317	0.828	229.13	180.89	22.425	0.583	62.25	425.15	22.629	0.978
129.57	456.40	22.318	0.663	255.61	342.40	22.430	0.867	181.36	159.22	22.629	0.416
27.50	184.22	22.319	0.622	58.51	400.70	22.430	0.933	214.09	324.59	22.658	-0.131
246.73	320.67	22.320	0.901	138.66	206.07	22.439	0.837	5.53	454.29	22.661	1.369
64.15	363.85	22.323	1.222	183.66	242.69	22.439	0.904	48.06	310.23	22.668	1.284
138.84	423.03	22.326	1.120	110.07	80.83	22.441	0.335	264.69	193.67	22.690	1.806
182.05	360.51	22.333	0.895	208.66	280.41	22.446	0.753	148.89	446.40	22.711	0.479
256.89	347.70	22.335	0.477	147.61	223.09	22.453	0.724	305.28	132.98	22.712	0.621
311.92	271.14	22.344	0.885	260.83	193.29	22.457	0.929	263.18	205.08	22.722	0.265
123.43	456.57	22.347	0.382	311.81	198.56	22.461	1.213	307.77	91.52	22.740	1.071
84.19	130.16	22.348	1.394	197.03	388.87	22.461	0.833	244.31	222.33	22.753	0.830
105.64	204.33	22.351	1.141	133.61	215.66	22.463	0.566	98.26	255.85	22.757	0.552
229.48	156.95	22.353	1.399	69.32	319.58	22.467	1.135	271.07	89.63	22.759	0.951
165.58	317.03	22.355	0.884	59.03	335.44	22.467	0.727	217.77	321.79	22.769	0.525
5.73	144.44	22.356	0.545	31.11	484.11	22.468	1.171	126.39	279.49	22.780	0.748
131.15	476.02	22.357	0.591	100.59	478.00	22.468	1.195	82.31	368.21	22.845	1.310
76.73	437.74	22.360	1.013	206.02	179.90	22.468	0.983	309.63	107.71	22.884	0.535
123.43	429.70	22.361	1.176	157.33	142.60	22.483	0.777	266.53	219.87	22.899	0.976
13.03	310.23	22.362	0.668	231.85	257.02	22.487	1.018	228.54	492.14	22.910	1.175
24.00	172.07	22.364	1.144	199.66	358.56	22.488	1.028	161.20	170.96	22.915	0.172
115.57	297.81	22.366	1.071	132.45	299.64	22.488	0.851	305.48	151.43	22.981	0.634
130.53	194.11	22.368	0.540	47.05	110.54	22.497	0.739	58.77	456.54	22.988	0.434
118.11	397.02	22.373	0.891	175.17	416.54	22.498	0.804	311.25	290.61	22.989	-0.123
297.47	37.26	22.375	1.061	54.40	249.80	22.540	0.942	247.48	342.82	23.026	1.620
69.34	385.63	22.377	0.548	22.03	275.51	22.548	0.998	184.14	302.44	23.028	0.917
119.40	60.34	22.382	1.172	94.54	317.96	22.562	0.879	164.65	24.59	23.138	0.494
183.01	222.16	22.383	0.749	198.04	67.38	22.566	1.219				

TABLE 3

M30 Main-Sequence Fiducial

V	$B-V$
17.2	0.624
17.4	0.612
17.6	0.600
17.8	0.572
18.0	0.506
18.2	0.437
18.4	0.413
18.6	0.410
18.8	0.413
19.0	0.418
19.2	0.424
19.4	0.437
19.6	0.455
19.8	0.474
20.0	0.494
20.2	0.519
20.4	0.542
20.6	0.572
20.8	0.609
21.0	0.643
21.2	0.685
21.4	0.725
21.6	0.766
21.8	0.805
22.0	0.840
22.2	0.875
22.4	0.913

was able to conclude that any metallicity variation among the main-sequence stars was limited to $[M/H] < 0.20$. We are unlikely to be able to set as stringent a limit with our data as the crowding is much more severe in our case. Since any metallicity inhomogeneity that does exist might be expected to be more pronounced in the inner regions of the cluster, we examine below the width of the main sequence in our field. The procedure is as follows. (1) Assume that the entire width of the main sequence is due to measurement error and chemical inhomogeneity for elements heavier than helium. This means that we exclude the possibility that binaries contribute to the spread in $(B-V)$ at a given value of V. (2) Calculate the dispersion in $(B-V)$ around the main-sequence fiducial in bins 0.2 mag wide in V ($\sigma_{\rm obs}$). This represents the observed width of the cluster main sequence. (3) Calculate the expected dispersion in $(B-V)$ from the errors in the photometry as returned by DAOPHOT ($\sigma_{\rm exp}$). Since there is some evidence that DAOPHOT somewhat underestimates the true errors (Bolte 1987*a*), particularly for faint stars, this procedure results in an eventual overestimate of the intrinsic width of the cluster main sequence. Hence, in reality, we will be calculating only an upper limit to the true chemical inhomogeneity of the cluster. (4) Calculate the true width $\sigma_{\rm int}$ of the main sequence, defined as $\sigma_{\rm obs} - \sigma_{\rm exp}$. This procedure yields the results listed in Table 4. This true width (actually an upper limit) can then be compared with models to estimate $\Delta[M/H]$.

TABLE 4

INTRINSIC WIDTH OF M30 MAIN SEQUENCE

$V(\pm 0.1)$	σ_{exp}	σ_{obs}	σ_{int}
18.1	0.014	0.031	0.028
18.3	0.013	0.017	0.011
18.5	0.015	0.019	0.012
18.7	0.014	0.015	0.005
18.9	0.024	0.019	...
19.1	0.017	0.021	0.012
19.3	0.016	0.029	0.024
19.5	0.023	0.019	...
19.7	0.023	0.036	0.028
19.9	0.024	0.036	0.027
20.1	0.028	0.046	0.036
20.3	0.032	0.030	...
20.5	0.036	0.051	0.036
20.7	0.034	0.062	0.052
20.9	0.045	0.059	0.038
21.1	0.051	0.070	0.048
21.3	0.054	0.101	0.085
21.5	0.059	0.095	0.074
21.7	0.068	0.106	0.081
21.9	0.078	0.071	...
22.1	0.085	0.073	...
22.3	0.096	0.059	...

In the region of the cluster turnoff ($M_V = 4.0$), the VandenBerg and Bell (1985) models predict that for metal-poor stars $\Delta(B-V)/\Delta[M/H] = 0.047$ magnitudes per dex while it is 0.030 near $M_V = 5.5$. These estimates assume that ΔY is zero. Using our turnoff values from Table 4 ($V \approx 18.6$) yields $\Delta[M/H] = 0.2$, while the fainter photometry results in the much less sensitive value $\Delta[M/H] = 1.2$. Both of these are upper limits to the true inhomogeneity for the reasons discussed above. Using only the result for stars near the turnoff, we can conclude that any chemical inhomogeneity in the cluster must be small, that it is not inconsistent with zero, and that there is no evidence that the regions closer to the center are any more inhomogeneous than those farther out (see Bolte 1987*a*).

We can also set a very stringent limit on any chemical abundance gradient in the cluster between 21 core radii (our field) and 65 core radii (Bolte's fields) by examining in detail the locations of the CMD fiducials in the two regions. In this discussion we assume that the absolute calibration of the photometry in both cases is "perfect," that is, there are no systematic sources of error in either data set. A comparison between the fiducials derived by Bolte and us is given in Figure 3 where the open circles are Bolte's data and the closed are ours. The two fiducials are in remarkably good agreement from the turnoff region through $V = 21.5$. Fainter than this our data tend to lie to the blue of Bolte's. Over the range $V = 18.3$ through 21.0 our sequence lies, on average, 0.004 mag redder

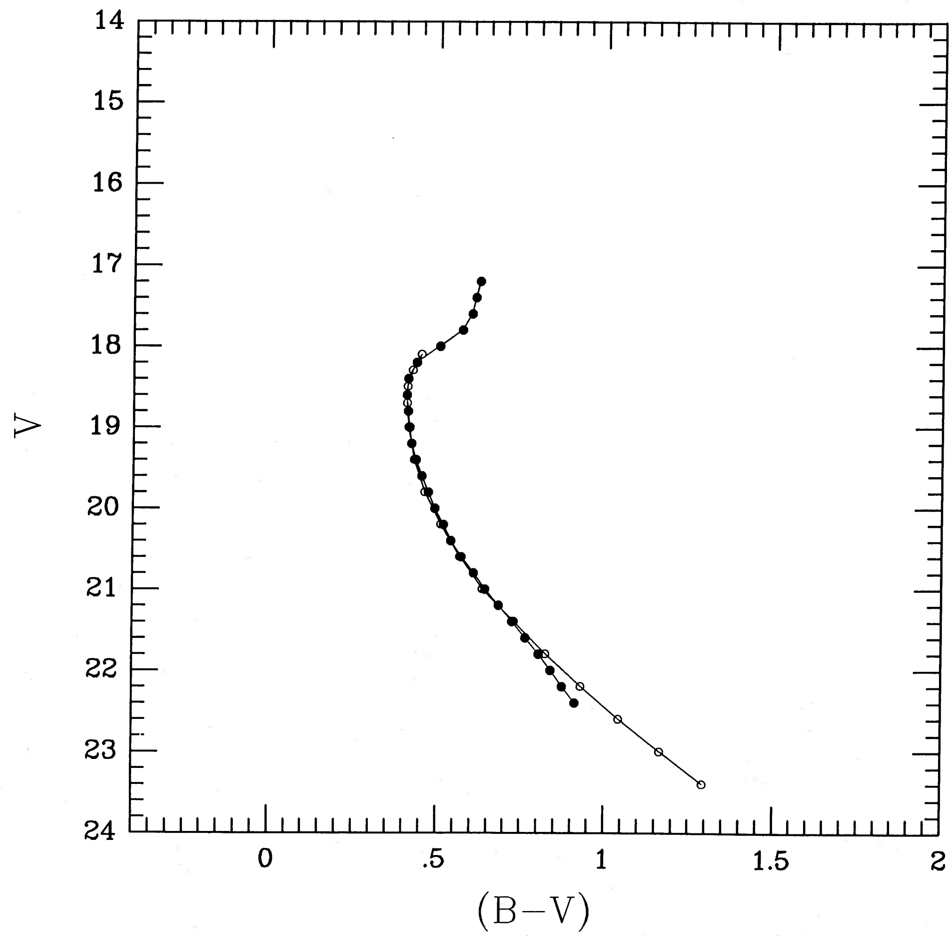

FIG. 3.—Fiducial sequences in M30 from a field at 21 core radii (*closed circles*, this paper), and one at 65 core radii (*open circles*, data from Bolte [1987*a*])

than that of Bolte's. Of course, all of this is easily attributable to a slight difference in the zero-point calibrations of the two data sets. However, if we assume that it establishes an upper limit to the metallicity difference between the two fields, we formally derive that the inner region is at most 0.09 dex more metal-rich than the outer one.

III. FUNDAMENTAL CLUSTER PARAMETERS

a) *Metal Abundance*

One of the fundamental parameters for M30 that our data set does not allow us to determine is the cluster metal abundance. The reason for this is that our U frames [from which we could determine $\delta(U-B)_{0.6}$ and hence an abundance estimate] were taken during the course of another program and are not deep enough to reach main-sequence stars with small errors. These frames will be used only to determine the cluster reddening from the horizontal branch stars. The metal abundance of M30 is, however, not controversial. Zinn and West (1984) have recently derived a value of $[M/\mathrm{H}] = -2.13$, while an earlier result based on ΔS measurements of two cluster RR Lyraes yielded -1.96 (Butler 1975). The recent compilation of globular cluster properties by Webbink (1985) records a value of -2.19. In our comparisons below with theoretical stellar models we will hence use those on the VandenBerg and Bell grid (1985) with $[M/\mathrm{H}] = -2.25$ and an enhanced oxygen abundance (VandenBerg 1988*a*) which seems to be required by the observations (Pilachowski, Sneden, and Wallerstein 1983).

b) *Reddening*

The M30 reddening has not been well established by previous studies. Zinn (1980) derives $E(B-V) = 0.01$, while Dickens (1972) suggests 0.06. Alcaino and Liller (1980) obtain 0.02 and Webbink (1985), relying mainly on the Dickens value, tabulates $E(B-V) = 0.06$ for M30. Our observations in U, B, and V are precise enough for stars brighter than the turnoff so that we can use the blue horizontal branch stars to obtain the reddening. The observations for these stars are listed in Table 5. If we place these stars in a color-color diagram and use the Population I fiducial found in Johnson (1966), we derive a redding for the M30 horizontal branch stars of $E(B-V) = 0.068 \pm 0.035$, in good agreement with the early value of Dickens, but in considerable disagreement with most other determinations. In the ensuing discussion we will adopt the value derived here, keeping in mind that all subsequently determined properties of M30 strongly depend on its reddening.

c) *Distance*

To determine the distance to M30, we adopt the procedure that we have been following in this series of papers, namely fitting a sequence of local subdwarfs to the observed main-sequence cluster fiducial The subdwarfs we will use are the same ones which we discussed earlier (Fahlman, Richer, and VandenBerg 1985), though HD 140283 has been dropped from the sample since Magain (1985) has recently shown that this star is actually a subgiant. For the remaining six stars, we have adopted the revised parallax data and Lutz-Kelker statistical corrections given by Lutz, Hanson, and van Altena (1987). After adjusting the observed colors of the subdwarfs to take into account the metallicity difference between an individual subdwarf and M30 and applying the reddening of 0.068 in $(B-V)$, the subdwarfs were fitted to the M30 fiducial by minimizing the differences in a least squares sense. This resulted in an apparent distance modulus to M30 of $(m-M)_V = 14.85 \pm 0.15$. This best fit of the subdwarfs to the M30 CMD is illustrated in Figure 4. The distance modulus that we derive here is larger than Bolte's value by 0.2 mag. The major reason for this is our higher reddening. He adopted $E(B-V) = 0.02$, 0.05 less than the result which we obtained. Our derived apparent distance modulus, together with the apparent magnitude of the horizontal branch ($V = 15.20$, Dickens 1972; Gratton 1985; Buonanno, Corsi, and Fusi Pecci 1987) leads to an absolute magnitude for the horizontal branch of $M_V = 0.35$, somewhat on the bright side.

TABLE 5

PHOTOMETRY OF HORIZONTAL BRANCH STARS

X, Y	V	$B-V$	$U-B$
138, 92	15.353	0.119	0.030
172, 152	15.393	0.069	−0.028
172, 273	15.475	0.044	−0.050
29, 127	15.553	0.038	−0.030
277, 151	15.598	0.045	−0.112
203, 266	15.729	−0.012	−0.170
208, 337	15.889	−0.056	−0.183
220, 336	16.045	−0.076	−0.339

d) *Helium Abundance*

The cluster helium abundance cannot be directly determined from our data. However, recent reviews (Yang *et al.* 1984; Boesgaard and Steigman 1985) suggest a primordial value for Y near 0.23, and this should set a lower limit to the initial globular cluster helium content. In addition, the study of numerous metal-poor emission-line galaxies (e.g., Kunth 1986) suggests $Y = 0.24$ for the primordial helium value. The best method of determining Y in globular clusters, the so-called R method, yields a mean value of 0.23 ± 0.02 (Buzzoni *et al.* 1983). Using this method, Dickens showed that M30 may have a higher helium abundance than most other clusters. In fact, if we apply the Buzzoni *et al.* relation between Y and R, and use Dickens's determination of R for M30, a value for Y near 0.27 is derived. Some further evidence that M30 may be somewhat helium-rich can be found in § IV*b* where we compare the observed location of the M30 horizontal branch with zero-age horizontal branch models containing different helium abundances. In the comparisons between theory and observation discussed below, however, the models will always have $Y = 0.24$, but the possibility of enhanced helium should be kept in mind.

IV. THE AGE OF M30

a) *Age Comparison with Other Metal-Poor Clusters*

An important aspect of the age question which can be examined without recourse to stellar models is whether or not there are significant cluster-to-cluster variations in age among the globulars having similar metallicities. This is an important question which bears on the collapse time of the Galaxy and the formation time scale of the cluster system. In a recent study of the available photometric data for 26 globular clusters, Gratton (1985) has suggested that those systems in the inner halo of the Galaxy, having galactocentric distances $R_g < 15$ kpc, are probably coeval, but that the age spread (in a given metallicity regime) could be as large as 3 Gyr. He also found that the outer halo clusters tend to be younger by up to 5 Gyr,

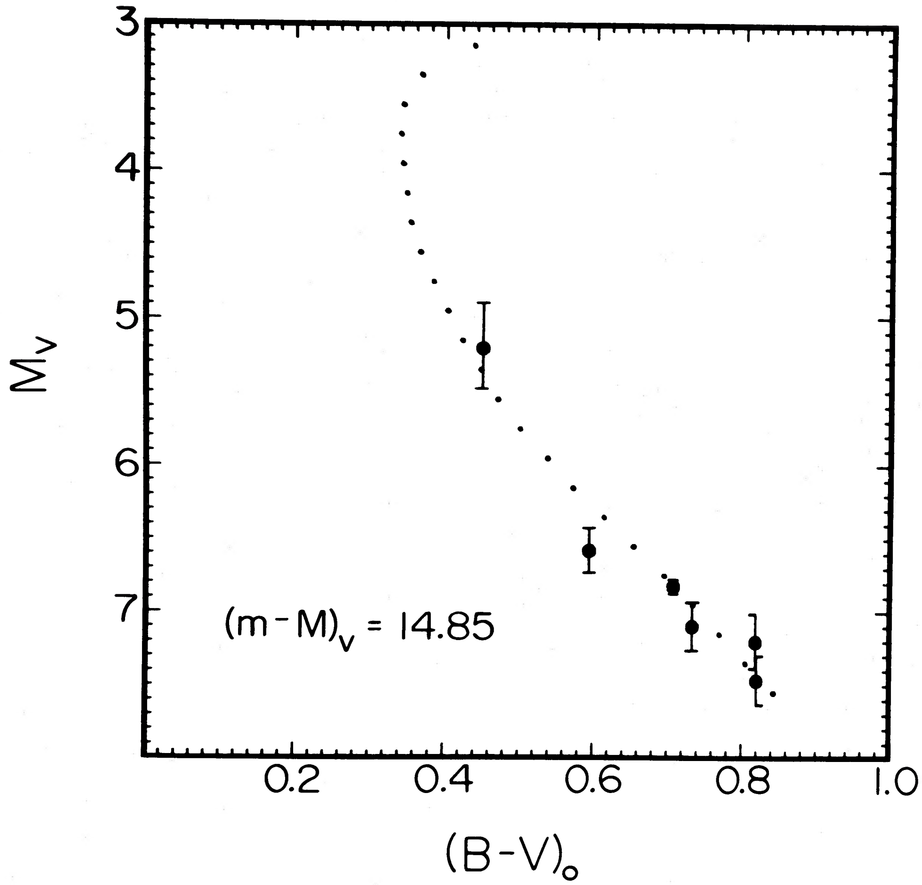

FIG. 4.—Best fit of local subdwarfs (*filled circles*) to the M30 CMD (*dotted curve*). The colors of the subdwarfs were adjusted so that they effectively have the same [M/H] as M30. The subdwarfs were then reddened by 0.068 mag in $(B-V)$ and fitted to the M30 fiducial by minimizing the square of the residuals in the vertical direction only. The derived distance modulus is $(m-M)_V = 14.85 \pm 0.15$. The error bars on the subdwarfs represent the 1 σ uncertainties of the stellar parallaxes.

though it now appears likely that problems with the data have led to his excessively young age estimates for the most distant globulars (see VandenBerg 1988*b*).

Since new CCD observations presently exist for M15 (Fahlman, Richer, and VandenBerg 1985), and for M68 (McClure *et al.* 1987)—two clusters whose metal abundances on the Zinn and West (1984) scale are within $\Delta[M/H] = \pm 0.04$ dex of that given for M30—an intercomparison of the CMDs for these three systems should be particularly instructive. To carry out this comparison we plot in an $M_V-(B-V)_0$ diagram the fiducial sequences for each cluster. The apparent distance moduli for all three clusters were determined strictly empirically by fitting the revised subdwarf sequnce to the respective lower main-sequence fiducials. This yields distance moduli of 15.29, 14.85, and 15.20 for M15, M30, and M68. The reddenings of M15 and M30 were also determined empirically from their respective color–color diagrams and the adopted values here are 0.11 and 0.068. The reddening of M68 was taken to be 0.07 (McClure *et al.* 1987). Figure 5 contains the comparison plot of these three fiducials. In general, the agreement between all these three clusters is remarkably good.

As can be seen in Figure 5, the M30 locus at the turnoff lies about 0.01 mag to the blue of that of M68, while that for M15 lies redward of M68's by about the same amount. This makes the M30 turnoff appear bluer and somewhat brighter than that of M68, and makes M15's somewhat redder and fainter. Thus, at first sight, one might be tempted to conclude from this that M30 is somewhat younger than M68, while M15 is somewhat older. However, it should be kept in mind that the reddenings of M15 and M30 are uncertain by about ± 0.04 so that the small differences, noted are well within the errors. In fact, if we arbitrarily reduce the reddening of M30 by 0.016 mag to 0.052 (well within the errors), then the M68 and M30 fiducials will overlay each other perfectly! Further, the differences seen near the turnoffs can equally well be explained as minor errors in the assigned distance moduli, particularly as the sense of the differences seen near the turnoffs are reflected in the differences seen at the horizontal branches. For example, relative to M68, if the M30 distance modulus were decreased by 0.15 mag and that for M15 increased by about the same amount, then both the main sequences and horizontal branches of all three clusters would overlap almost perfectly. These changes are all within the 1 σ errors of the distances to these clusters.

If we decide, however, to accept Figure 5 at face value, then either M30 is more metal-poor than M68 or it is younger, while either M15 is more metal-rich than M68 or it is older. We can set limits to these differences by using the models of VandenBerg and Bell (1985) differentially. Assuming first that M15, M30, and M68 all have the same age, and attributing the color differences entirely to a metallicity effect, then, as we discussed in § II, $\Delta(B-V)/\Delta[M/H] = 0.047$ mag per dex for stars near the turnoff. The 0.01 mag color difference between M30 and M68 then implies that M30 is more metal-poor than M68 by about 0.21 dex, while M15 is more metal-rich by the

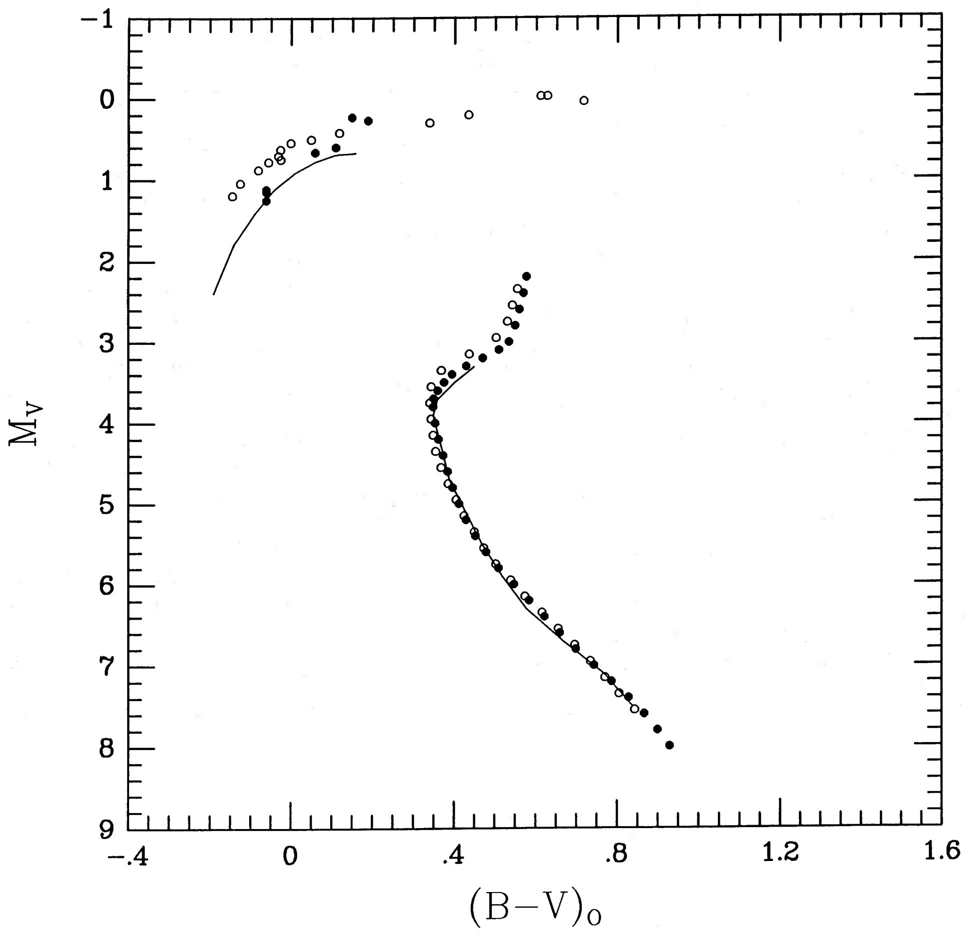

FIG. 5.—Comparison of the color magnitude diagrams of three metal-poor clusters: M15 [*continuous line*, $(m-M)_V = 15.29$, $E(B-V) = 0.11$]; M30 [*open circles*, $(m-M)_V = 14.85$, $E(B-V) = 0.068$]; and M68 [*closed circles*, $(m-M)_V = 15.20$, $E(B-V) = 0.07$].

same amount. Alternately, if the apparent bluer and brighter turnoff of M30 relative to M68 is caused solely by a younger age, then the models predict that this age difference is about 2 Gyr, while, similarly, M15 would be about 2 Gyr older than M68.

Another parameter which reflects on the ages of these systems is the magnitude difference between the horizontal branch and the turnoff (Sandage 1982). It is somewhat difficult to define precisely this quantity because of the vertical morphology of the turnoff region and the upward slope of the horizontal branch. These effects introduce an uncertainty of about ± 0.2 mag in this quantity which translates to an uncertainty in the age of ± 3 Gyr. These magnitude differences are 3.3, 3.4, and 3.5 respectively for M15, M30, and M68. Within the errors, there is no evidence that the magnitude differences between the horizontal branches and the turnoffs for these clusters are different.

To summarize then, a comparison of the fiducial sequences of M15, M30, and M68 indicates that, to within the errors, the clusters can certainly have identical metallicities and ages. If we interpret the slight color differences as a metallicity variation only, then M30 is about 0.21 dex more metal-poor than M68, while M15 is more metal-rich than M68 by this same amount. If we view the slight differences in their main sequence fiducials as an age spread, then M30 is about 2 Gyr younger than M68, while M15 is 2 Gyr older. These numbers can be taken as a good indication of the real uncertainty in the *relative* ages of metal-poor clusters.

b) *Isochrone Fits to the M30 CMD*

In order to estimate the absolute age of M30, it is necessary to compare the data with the most appropriate set of theoretical isochrones that is presently available. The procedure that we have used throughout the present series of papers will also be employed here. That is, the various free parameters which have an impact on the fit will be determined empirically prior to making the comparison with the theory so that the selection of the particular isochrone that is implied by the data is constrained as much as possible.

For the cluster reddening we adopt 0.068 (see § III). As shown in Figure 4, the distance from the subdwarf fit that is consistent with this reddening corresponds to $(m-M)_V = 14.85$. We adopt $Y = 0.24$ and $[M/H] = -2.13$ for M30 (see § III). Finally, theoretical calculations (e.g. Rood 1981; VandenBerg 1985) have demonstrated that predicted turn-off luminosities and temperatures (and hence inferred ages) depend sensitively on the oxygen abundance, which probably does not scale with the iron content. While the oxygen abundance in M30 is not presently known, analysis of metal-poor field stars (see the review by Sneden 1985) lead us to expect that the cluster [O/Fe] value is likely somewhere in the range from +0.5 to +1.0. Based on the latest observations (Gratton and Ortolani 1986) and models of galactic chemical evolution (Matteucci 1986), there may be some preference for $0.5 \leq [O/Fe] \leq 0.7$.

The set of isochrones which comes closest to satisfying the above constraints on chemical composition is that for $Y = 0.24$, $[M/H] = -2.25$, and $[O/Fe] = 0.5$, which was computed by VandenBerg (1985). In all respects, other than the differences in assumed abundances, these models are identical to those presented by VandenBerg and Bell (1985). That is, they were computed using the same evolutionary code and employed the same transformation relations to pass from the theoretical to the observational plane. Figure 6 illustrates that these isochrones provide a very fine fit to the M30 CMD. Note that, in order for them to reproduce the observed lower main sequence, the theoretical curves had to be shifted to the red by the indicated 0.03 mag. Why such a correction is necessary (here, and in almost all other studies which have used the VandenBerg-Bell generation of isochrones) has yet to be satisfactorily explained, but presumably the discrepancy is indicating a problem with the model colors or temperatures. Work to resolve the source of this color shift, such as comparing complementary observations at infrared wavelengths (for instance) with the relevant isochrones, should be given high priority.

This matter aside, it is clear that the detailed shape of the observed locus is reproduced to high accuracy by the models for an age close to 14 Gyr. What is particularly encouraging is that the derived distance is such that near consistency is also achieved between the predicted and the observed location of the zero-age horizontal branch (ZAHB) which thereby argues in favor of the interpretation of the data which we have found. The fact that the observed locus of the horizontal branch lies somewhat brighter than the ZAHB is to be expected as recent horizontal branch evolutionary models (Lee, Demarque, and Zinn 1987) predict that in metal-poor clusters HB stars just to the red of the RR Lyrae gap should be populated by evolved stars which are above the ZAHB at that color.

During the preparation of this paper, we became aware of the parallel study of M30 by Bolte (1987*a*) who also used oxygen-enhanced isochrones in his analysis but found an age of 17 Gyr which seems inconsistent with Figure 6. However, Bolte adopted $E(B-V) = 0.02$ mag, and therefore, on the basis of the subdwarfs, derived a much shorter distance modulus $[(m-M)_V = 14.65]$ than that which we obtained. As a result, a high age was the natural outcome of the isochrone fit in his case. Bolte made no use of the fit to the horizontal branch in his comparison with the theory. If he had chosen to include the observed horizontal branch and the theoretical ZAHB models discussed in McClure *et al.* (1987) in his fits, he would have discovered that a distance modulus as small as 14.65 places the theoretical ZAHB somewhat above the observed horizontal branch. This contradiction provides a fairly strong argument that the cluster distance modulus must

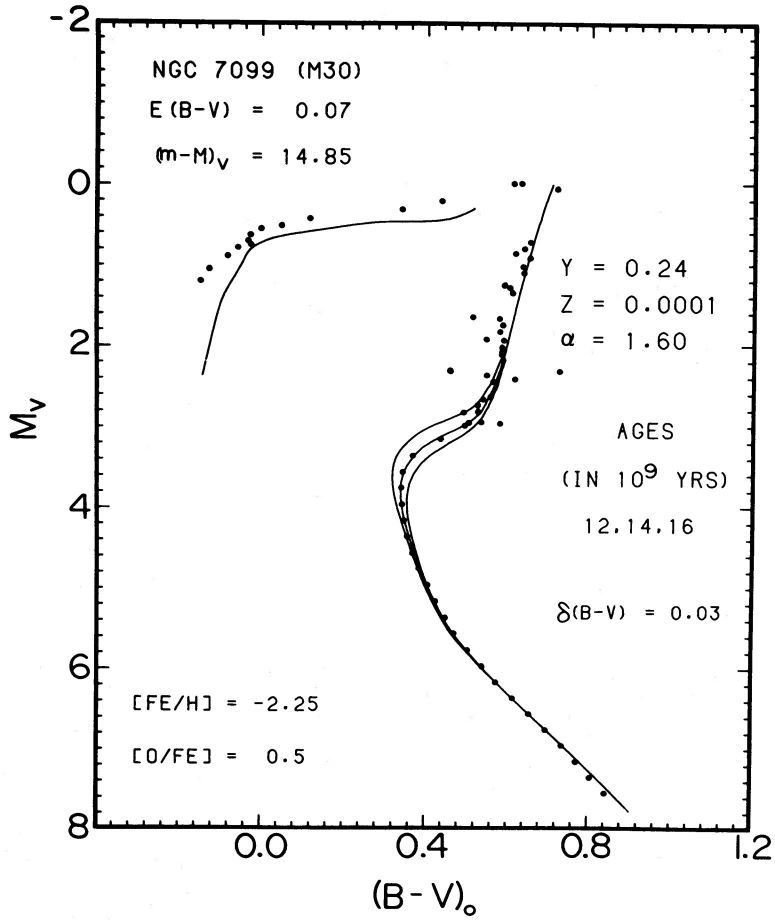

FIG. 6.—An overlay (not a fit) of the VandenBerg (1985) oxygen-enhanced isochrones onto the M30 CMD. The isochrones were reddened by 0.068 mag in $(B-V)$ and shifted so that they represent a cluster with an apparent V distance modulus of 14.85 mag.

be at least somewhat larger than $(m-M)_V = 14.65$ mag. However, we have shown that Bolte's photometry agrees with ours. Had he interpreted his data in the same way as us, he would have gotten the same result that we obtained.

Figure 7 illustrates the effects on the models and hence on the interpretation of the M30 observations of changing, on the one hand, the adopted [O/Fe] ratio, and on the other, the assumed helium content. The effects of varying the oxygen abundance have already been discussed in some detail by VandenBerg (1985), but it is useful to emphasize the main points. First the predicted location of the turnoff depends sensitively on the oxygen content in the sense that the higher the [O/Fe] ratio, the younger the age corresponding to a given turn-off luminosity. In the example shown, it is clear that the 14 Gyr isochrone for [O/Fe] = 0.0 is too bright while that for [O/Fe] = 1.0 is too faint in comparison with the data. Consequently, had we assumed a lower or a higher value of [O/Fe], we would have obtained a larger or smaller age, respectively, by about 1.5–2 Gyr for a change in [O/Fe] of 0.5 dex. This assumes, of course, that the apparent distance modulus is fixed at a value of 14.85. The second important ramification of enhanced oxygen is that high [O/Fe] causes the red end of a computed ZAHB to be shifted to lower luminosity and effective temperature (Castellani and Tornambé 1977). While the present M30 observations cannot discriminate between the three theoretical loci (the two reddest stars could well be entering their asymptotic giant branch phase of evolution), a larger data sample might well offer some potential in this regard. Note that the blue end of the ZAHB is not affected by variations in [O/Fe] so that distances based on fits of models to the distribution of stars with $(B-V)_0$'s ≤ 0.2 will be independent of this uncertainty. However, the luminosities of RR Lyrae stars, which have redder colours by about 0.1 mag or so, will be a function of their oxygen content. Hence the magnitude difference between metal-poor and metal-rich RR Lyraes will clearly depend on how [O/Fe] scales with [Fe/H].

The right hand panel of Figure 7 shows that the effects of varying Y are less important at the turnoff than at the horizontal branch. In fact, if the distance which we have derived for M30 is accurate, the cluster helium content as measured from

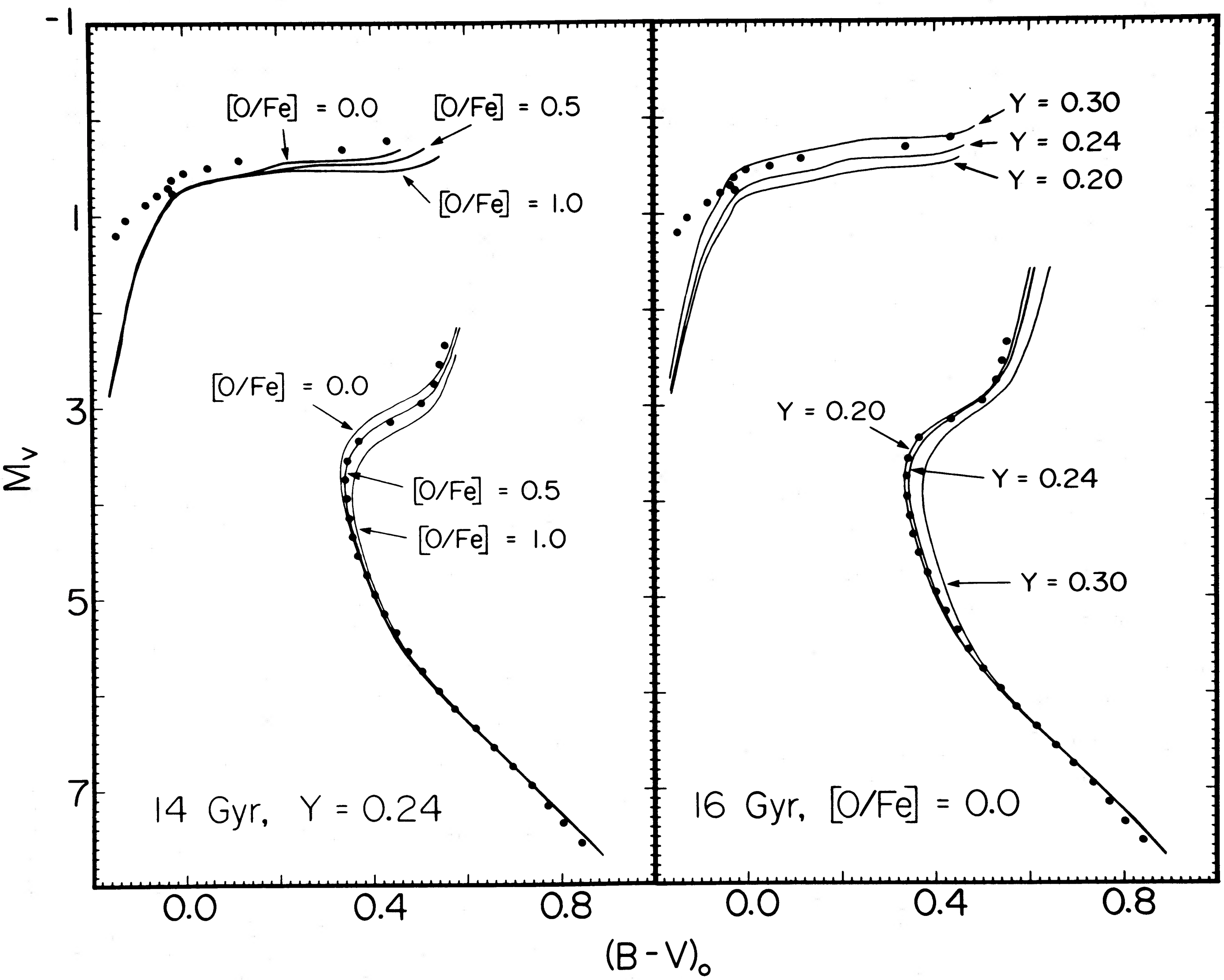

FIG. 7.—The effect on the interpretation of the M30 observations of changing the [O/Fe] ratio in the models (*left-hand panel*), and the helium content (*right-hand panel*)

1988ApJ...329..187R

the main-sequence stars is constrained to a value which is close to $Y = 0.24$. A helium abundance as high as $Y = 0.30$ is clearly ruled out since the observed location of the mean horizontal branch is fainter than the computed ZAHB (a contradiction), while the theoretical ZAHB for $Y = 0.20$ is much too faint for the assumed distance. Indeed, the models at both the horizontal branch and the turnoff suggest that the initial cluster helium content is probably somewhere in the range $0.23 \leq Y \leq 0.27$.

Hesser *et al.* (1987) have recently completed a study of 47 Tuc and have found, using a set of oxygen-enhanced models, an age close to 14 Gyr. In view of the present findings for a similar age for the metal-poor globular clusters (here we include the results also for M15 and M68), it appears that if there is an age-metallicity relation among the globulars, it must be moderately small; the entire range not exceeding about 4 Gyr.

The temptation to use these new cluster ages to constrain the age of the universe and the Hubble constant H is, of course, irresistible. If we take 14 Gyr as the age of the universe and adopt $\Omega = 1.0$ and $\Lambda = 0$, the Hubble constant must then be 48 km s^{-1} Mpc^{-1}.

V. THE LUMINOSITY FUNCTION OF M30

The luminosity function (LF) of M30 is of interest for several reasons. First, being a metal-poor system, we can investigate whether the slope of its mass function is as steep as would be expected from the result of McClure *et al.* (1986). Second, the cluster has a collapsed core (King 1986) and thus can be considered to be dynamically quite evolved. For this reason it is important to compare our resulting LF (observed at 21 core radii) with that derived by Bolte (1987*b*) at a distance of ~ 65 core radii from the cluster center in order to investigate whether there is any evidence of dynamical relaxation. The signature of dynamical relaxation will be LFs that vary systematically with distance from the cluster center. The function closer to the cluster center will be flatter because the low-mass stars are preferentially driven outward as the cluster relaxes toward an equilibrium state. Bolte (1987*b*) showed that the mass spectral index x, defined by assuming that the differential mass distribution is $\Phi(m) \propto m^{-(1+x)}\, dm$, where $\Phi(m)$ is the number of stars with masses in the range m to $m + dm$, of M30 at 65 core radii is $x \approx 1.6$, in apparent reasonable agreement with the metallicity-x correlation found by McClure *et al.* (1986).

Since our V frames are deeper than those in B, we adopt the following procedure in deriving the cluster LF. (1) All stars present on the V frames at a level of at least 3.5 σ above the sky are included in the counts. After establishing this list of objects, *every* one was visually inspected on our image display system to ensure that it was stellar and not caused by bad pixels. The faint galaxy contribution to our counts (which extend only to $V = 23$) is negligible (Koo 1986). (2) Corrections for incompleteness were determined by adding stars of known magnitude into the frames and then rereducing them again in the normal manner. (3) The field star contribution was evaluated from published theoretical models of star counts in our Galaxy (Bahcall and Soneira 1980). No blank fields near M30 were obtained, but this is not a serious restriction as the field contamination is small. Table 6 contains the derived M30 LF. In this listing column (3) is the actual number of stars counted on the frame, column (5) the incompleteness and background corrected counts, and column (6) the logarithm of column (5).

Figure 8 illustrates a comparison of the observed LF of M30 with various theoretical loci that have been generated from the isochrone which best reproduces the cluster CMD (see Fig. 6), namely, that for an age of 14 Gyr. Error bars are included for each point, these errors including the uncertainty in the incompleteness corrections. It is apparent that, for the adopted distance modulus, the observations are very well represented by the theoretical LF for a mass spectral index of $x = 0$. Although additional comparisons were performed for different choices of age, distance, and composition, the result shown is insensitive to moderate changes in these parameters (e.g., varying the distance modulus by up to ± 0.2 mag had no effect on the value of x, in this sense the result seen in Fig. 8 is quite robust). All such comparisons indicated that the mass spectrum in the field surveyed in M30 must be very flat, with a value of x near zero. This apparently contrasts markedly with the case of M15 which is observed to have a steep mass function as indicated in Figure 8. However, the M15 data were secured at 95 core radii from the cluster center. The implication of this will be considered further below.

TABLE 6

M30 LUMINOSITY FUNCTION

V (1)	% Complete (2)	Number Counted (3)	Field (4)	$N(V)$ (5)	log $N(V)$ (6)
14–15......	100	8	0.3	7.7	0.89
15–16......	100	19	0.5	18.5	1.27
16–17......	100	13	0.8	12.2	1.09
17–18......	100	33	1.2	31.8	1.50
18–19......	100	171	1.9	169.1	2.23
19–20......	88	346	3.0	390.0	2.59
20–21......	80	533	3.9	662.4	2.82
21–22......	73	554	4.9	753.0	2.88
22–23......	34	280	6.1	806.7	2.91

As pointed out above, Bolte (1987*b*) found that $x \approx 1.6$ for his field in M30 located at 65 core radii, while we find $x = 0$ at 21 core radii. *This is clear evidence for mass segregation in this cluster.* We can use the multimass King-Mitchie models of Pryor, Smith, and McClure (1986) to investigate what these values imply for the global value of x. These authors investigated the effect of mass segregation acting on a global mass function in a globular cluster. The tidal and core radii of M30 (Webbink 1985) imply that the concentration parameter c (defined as the logarithm of the ratio of these two quantities) is about 2.3. (Although the core radius of M30 is not well defined by the King-Mitchie models as it has a central luminosity cusp [King 1986], we will nevertheless use the value for the core radius given by Webbink [1985] in the following discussion. The value quoted by Webbink is the best-fitting King-Mitchie value.) Pryor *et al.* provide models for clusters with $c = 2.2$, which should be a good approximation to M30. Figure 9 illustrates these models for this value of c. In this diagram, the abscissa is the *apparent* (i.e., observed) mass function slope and the ordinate is radial position in the cluster (in units of the core radius). The continuous curves plot the observed mass function exponents against radius for clusters with true mass function slopes of 0.0, 0.67, 1.35, and 2.0. The closed circle plotted in this diagram is our data point discussed above, while the open circle is Bolte's (1987*b*) value. A realistic error of ± 0.3 in x is indicated for each point.

The models of Pryor *et al.* seem to imply that the global mass function slope inferred from our inner point is about 0.0, while that derived from Bolte's value at 45 core radii is about

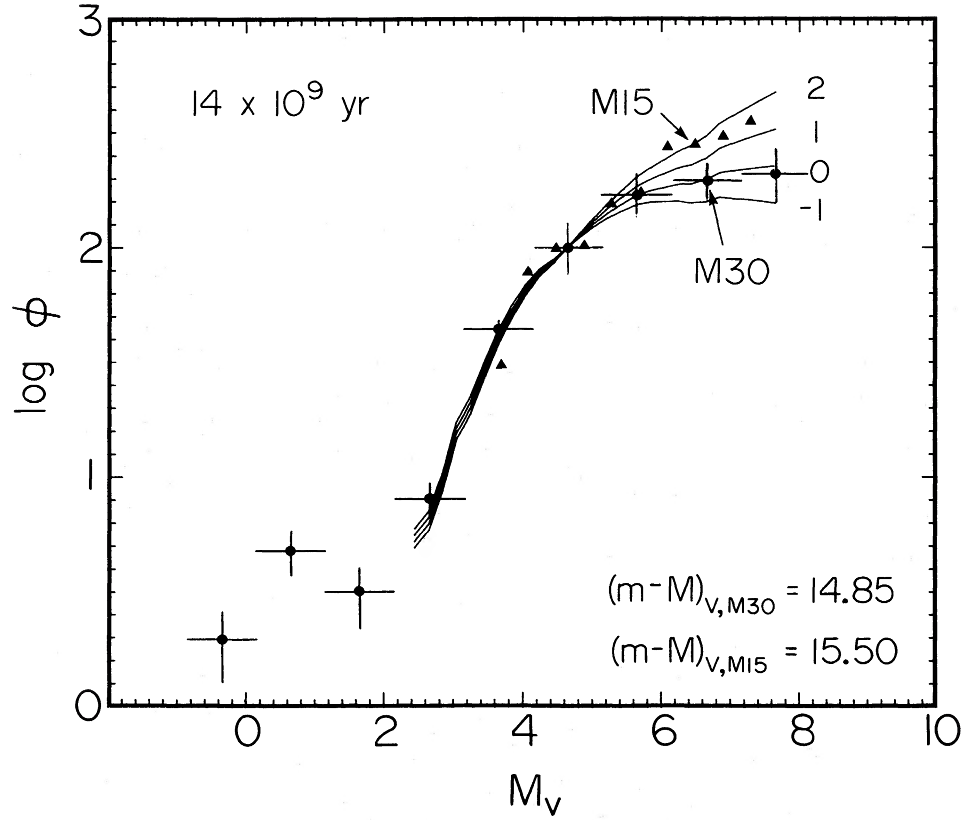

FIG. 8.—Comparison of our observed luminosity function of M30 (*closed circles*) with theoretical loci generated from the isochrone which best matches the cluster CMD. The error bars indicated include errors in the incompleteness corrections. Curves for mass function exponents, x, equal to -1.0, 0.0, 1.0, and 2.0 are shown. Data for M15 (which has a similar metal abundance) are also indicated. The M15 data were secured at 95 core radii from the cluster center. The large distance modulus used for M15 (0.2 mag larger than that indicated by the subdwarfs) is to force M15 to have the same age as M30 so that a single set of theoretical LF's could be placed in this diagram. This has no major effect on the resulting value of x, the mass spectral index.

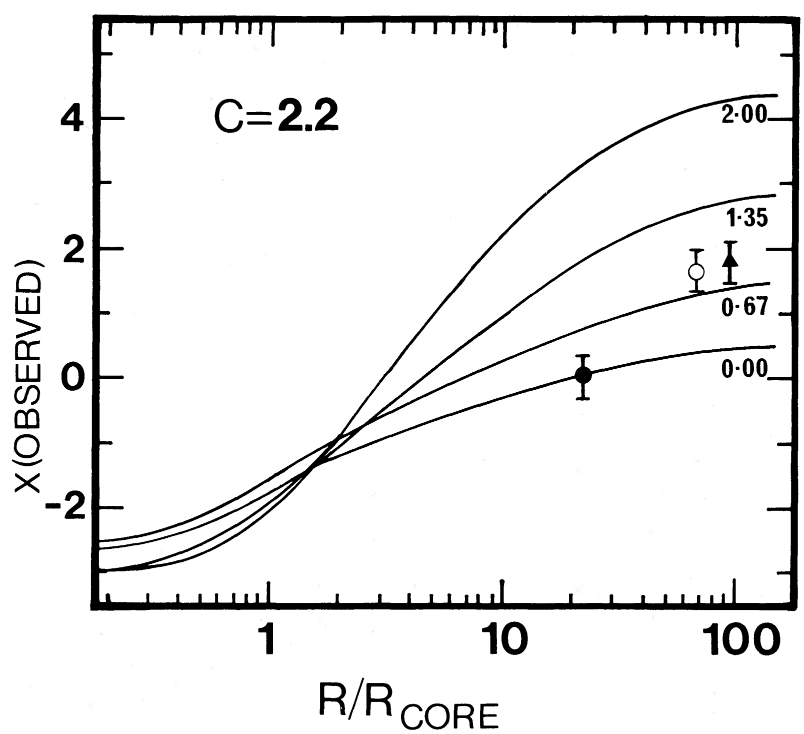

FIG. 9.—The effect of mass segregation on the global slope of the cluster mass function. The curves shown, taken from Pryor *et al.*, are for a cluster with $c = 2.2$ and x, the slope of the global power-law mass function, equal to 0.0, 0.67, 1.35, and 2.0. The Y axis is the *observed* slope, while the X axis is radial distance in units of the core radius. The closed circle is for M30 (this paper, 21 core radii), while the open circle is Bolte's M30 result (1987*a*, 65 core radii). The closed triangle is for M15 (Fahlman, Richer, and VandenBerg 1985, 95 core radii).

1.0. These two values are, at best, only marginally consistent with each other if our error of ± 0.3 for each point is realistic. Pryor *et al.* give numerous reasons in their paper why their multimass King-Mitchie models probably overestimate the corrections for mass segregation. However, the data discussed above suggest that the corrections may, in fact, be too small! This situation means that it is not possible for us to determine with any precision the global mass spectral index for M30. This is a very different situation from that which we encountered in our study of the luminosity function in M5 (Richer and Fahlman 1987). Here, good consistency was obtained for the global value of x in three fields at 8, 21, and 58 core radii. The concentration parameter for M5 is only slightly smaller than that for M30 and is equal to 1.9. Whether unusual clusters like M30 (collapsed core therefore very dynamically evolved, perhaps steep global mass spectral index) are just not well modeled by the King-Mitchie models discussed by Pryor *et al.*, or whether it is simply a problem with some of the assumptions involved in these models (e.g., a mass cutoff at 0.2 $M_\odot$), is not clear.

In this context, it is of interest to reexamine the existing data for the similar cluster M15. Both it and M30 are metal-poor, have collapsed cores, and are expected to have steep mass spectral indices from the result of McClure *et al.* (1986). Our new fit to the M15 data (taken from Fahlman, Richer, and VandenBerg) is shown in Figure 8 and implies that the observed mass function exponent has a value of x somewhere in the range of $1.5 \leq x \leq 2.0$, smaller than the original estimate of McClure *et al.* (1986), but consistent with a revised value given by McClure *et al.* (1988). Again, using the Pryor *et al.* models for $c = 2.2$ (a good approximation for M15 also), we can put in Figure 9 the data point for M15 plotted as a filled triangle. We see that, within the framework of the Pryor *et al.* models, a fair estimate of the global value of the mass function slope is $x \approx 0.9$, similar to that derived for the outer field in M30. Evidently a study of fields closer to the center of M15 would be very valuable here in order to investigate if a trend similar to that seen in M30 is found.

The main conclusion to be drawn from this discussion of the M30 LF is that the corrections for mass segregation in at least some extreme clusters (e.g. M15, M30) are not yet very well understood. Since it is precisely these clusters which tie down the low metallicity end of the x-metallicity relation found by McClure *et al.* (1986), the relationship found in that paper should be exposed to the widest possible tests including LFs of other very metal poor systems without collapsed cores. An excellent example in this category is NGC 5053 which is as metal-poor as M15 and M30 but is also one of the loosest clusters known with $c = 0.75$. The models of Pryor *et al.* predict that the dynamical corrections to the observed LF should be negligible. We are currently analyzing deep CCD data for this cluster. On the positive side, the results obtained here should be capable of providing useful constraints on dynamical models of post–core-collapse clusters.

VI. SUMMARY

New *UBV* CCD photometry in a single field of the globular cluster M30 was obtained at CFHT under conditions of good seeing (0".9). The data were used to obtain the color magnitude diagram of the cluster, its luminosity function, and to derive as many fundamental cluster parameters as the data allowed. The results which we obtained are as follows.

1. No blue stragglers, nor any evidence of a binary sequence is seen in the data even though the field in which we observed is only 3'.4 (21 core radii) from the cluster center. The main-sequence cluster stars were found to be highly chemically homogeneous, with an upper limit of about 0.20 dex to any spread in metal abundance.

2. The CMD fiducial sequences of three metal-poor clusters were intercompared with the aim of detecting any age differences among them. Within the errors in the cluster reddenings and distances there is no evidence for an age spread among these three clusters. If the small differences seen are interpreted as an age spread at constant metal abundance, then the three clusters have a total spread in ages of at most 4 Gyr. Alternatively, if these clusters have the same age, then the total metal abundance variation among them is 0.42 dex with M30 the most metal poor system of the three.

3. The age which we derive for M30 itself is 14 Gyr. The reduction in age here to 14 Gyr from the previous values of 16–18 Gyr for other globulars is due primarily to the assumption of enhanced helium (over the usually assumed value of $Y = 0.20$) and of enhanced oxygen. *This difference in age should not be interpreted as simply the scatter in the determinations.* Since the models are believed to be representative of cluster stars in so far as their abundances are concerned, and since there is excellent overall consistency of synthetic and observed CMDs (from $0 \leq M_V \leq 8$), we believe that a reasonable uncertainty in our age estimate is ± 2 Gyr. That is, it is possible, but not probable, that M30 is either younger than 12 Gyr or older than 16 Gyr.

4. The cluster luminosity function was measured, and the slope of the assumed power law mass function was found to be very flat with $x \approx 0.0$. The existing models of Pryor *et al.* for mass segregation corrections yield a global value of the slope of the mass function based on our inner field and one measured by Bolte about 3 times as far from the center that are not consistent. The observations seem to indicate that the mass segregation corrections implied by these models is too small, whereas Pryor *et al.* make a strong case for the opposite conclusion.

The authors are indebted to CFHT for the assignment of telescope time in support of their globular cluster research program. This research is supported by grants from the Natural Sciences and Engineering Research Council of Canada.

REFERENCES

Alcaino, G., and Liller, W. 1980, *A.J.*, **85**, 1330.
Bahcall, J. N., and Soneira, R. N. 1980, *Ap. J. Suppl.*, **44**, 73.
Boesgaard, A. M., and Steigman, G. 1985, *Ann. Rev. Astr. Ap.*, **23**, 319.
Bolte, M. J. 1987*a*, preprint.
———. 1987*b*, *Bull. AAS*, **19**, 676.
Buonanno, R., Corsi, C. E., and Fusi Pecci, F. 1985, *Astr. Ap.*, **145**, 97.
———. 1987, preprint.
Butler, D. 1975, *Ap. J.*, **200**, 68.
Buzzoni, A., Fusi Pecci, F., Buonanno, R., and Corsi, C. E. 1983, *Astr. Ap.*, **128**, 94.
Castellani, V., and Tornambé, A. 1977, *Astr. Ap.*, **61**, 427.
Dickens, R. J. 1972, *M.N.R.A.S.*, **157**, 299.
Fahlman, G. G., Richer, H. B., and VandenBerg, D. A. 1985, *Ap. J. Suppl.*, **58**, 225.
Gratton, R. G. 1985, *Astr. Ap.*, **147**, 169.
Gratton, R. G., and Ortolani, S. 1986, *Astr. Ap.*, **169**, 210.

Hesser, J. E., Harris, W. E., VandenBerg, D. A., Allwright, J. W. B., Shott, P., and Stetson, P. B. 1987, *Pub. A.S.P.*, in press.
Johnson, H. L. 1966, *Ann. Rev. Astr. Ap.*, **4**, 193.
King, I. 1986, in *IAU Symposium 113, Dynamics of Star Clusters*, ed. J. Goodman and P. Hut (Dordrecht: Reidel), p. 1.
Koo, D. C. 1986, *Ap. J.*, **311**, 651.
Kunth, D., 1986, *Pub. A.S.P.*, **98**, 984.
Landolt, A. U. 1983, *A.J.*, **88**, 439.
Lee, Y-W., Demarque, P., and Zinn, R. 1987, in *The Second Conference on Faint Blue Stars*, ed. A. G. D. Philip, D. S. Hayes, and J. Liebert (Schenectady: L. Davis Press), in press.
Lutz, T. E., Hanson, R. B., and van Altena, W. F. 1987, *Bull. AAS*, **19**, 675.
Lutz, T. E., and Kelker, D. H. 1973, *Pub. A.S.P.*, **85**, 573.
Magain, P. 1985, *Astr. Ap.*, **146**, 95.
Margon, B., and Downes, R. A. 1983, *Ap. J. (Letters)*, **274**, L31.
Matteucci, F. 1986, *Pub. A.S.P.*, **98**, 973.
McClure, R. D., Stetson, P. B., Hesser, J. E., Smith, G. H., Harris, W. E., and VandenBerg, D. A. 1988, in *IAU Symposium 126, Globular Cluster Systems in Galaxies*, ed. J. Grindlay and A. G. D. Philip (Dordrecht: Reidel), in press.
McClure, R. D., VandenBerg, D. A., Bell, R. A., Hesser, J. E., and Stetson, P. B. 1987, *A.J.*, **93**, 1144.
McClure, R. D., VandenBerg, D. A., Smith, G. H., Fahlman, G. G., Richer, H. B., Hesser, J. E., Harris, W. E., Stetson, P. B., and Bell, R. A. 1986, *Ap. J. (Letters)*, **307**, L49.
Pilachowski, C. A., Sneden, C., and Wallerstein, G. 1983, *Ap. J. Suppl.*, **52**, 241.
Pryor, C., Smith, G. H., and McClure, R. D. 1986, *A.J.*, **92**, 1358.
Richer, H. B., and Fahlman, G. G. 1987, *Ap. J.*, **316**, 189.
Rood, R. T. 1981, in *Physical Processes in Red Giants*, ed. I. Iben Jr. and A. Renzini (Dordrecht: Reidel), p. 51.
Sandage, A. 1982, *Ap. J.*, **252**, 553.
Sneden, C. 1985, in *Production and Distribution of C, N, O Elements*, ed. I. J. Danziger, F. Matteucci, and K. Kjär (Garching European Southern Observatory), p. 1.
Stetson, P. B. 1987, *Pub. A.S.P.*, **99**, 191.
VandenBerg, D. A. 1985, *Production and Distribution of C, N, O Elements*, ed. I. J. Danziger, F. Matteucci, and K. Kjär (Garching: European Southern Observatory), p. 73.
VandenBerg, D. A. 1988*a*, in preparation.
———. 1988*b*, in *IAU Symposium 126, Globular Cluster Systems in Galaxies*, ed. J. Grindlay and A. G. D. Philip (Dordrecht: Reidel), in press.
VandenBerg, D. A., and Bell, R. A. 1985, *Ap. J. Suppl.*, **58**, 561.
Webbink, R. F. 1985, in *IAU Symposium 113, Dynamics of Star Clusters*, ed. J. Goodman and P. Hut (Dordrecht: Reidel), p. 541.
Yang, J., Turner, M. S., Steigman, G., Schramm, K. A., and Olive, K. A. 1984, *Ap. J.*, **281**, 493.
Zinn, R. 1980, *Ap. J. Suppl.*, **42**, 19.
Zinn, R., and West, M. J. 1984, *Ap. J. Suppl.*, **55**, 45.

GREGORY G. FAHLMAN and HARVEY B. RICHER: Department of Geophysics and Astronomy, University of British Columbia, No. 129-2219 Main Mall, Vancouver, B.C. V6T 1W5, Canada

DON A. VANDENBERG: Department of Physics, University of Victoria, P.O. Box 1700, Victoria, B.C. V8W 2Y2, Canada